

111-02
57029
21 p.

A New Algorithm for Five-Hole Probe Calibration, Data Reduction, and Uncertainty Analysis

Bruce A. Reichert and Bruce J. Wendt
Lewis Research Center
Cleveland, Ohio

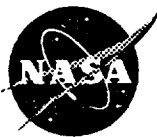
(NASA-TM-106458) A NEW ALGORITHM
FOR FIVE-HOLE PROBE CALIBRATION,
DATA REDUCTION, AND UNCERTAINTY
ANALYSIS (NASA. Lewis Research
Center) 21 p

N95-12378

Unclass

G3/02 0027029

September 1994



National Aeronautics and
Space Administration

A NEW ALGORITHM FOR FIVE-HOLE PROBE CALIBRATION, DATA REDUCTION, AND UNCERTAINTY ANALYSIS

Bruce A. Reichert and Bruce J. Wendt*
Internal Fluid Mechanics Division
NASA Lewis Research Center
Cleveland, Ohio

ABSTRACT

A new algorithm for five-hole probe calibration and data reduction using a non-nulling method is developed. The significant features of the algorithm are: 1) two components of the unit vector in the flow direction replace pitch and yaw angles as flow direction variables, and 2) symmetry rules are developed that greatly simplify Taylor's series representations of the calibration data. In data reduction, four pressure coefficients allow total pressure, static pressure, and flow direction to be calculated directly. The new algorithm's simplicity permits an analytical treatment of the propagation of uncertainty in five-hole probe measurement. The objectives of the uncertainty analysis are to quantify uncertainty of five-hole probe results (e.g., total pressure, static pressure, and flow direction) and determine the dependence of the result uncertainty on the uncertainty of all underlying experimental and calibration measurands. This study outlines a general procedure that other researchers may use to determine five-hole probe result uncertainty and provides guidance to improve measurement technique. The new algorithm is applied to calibrate and reduce data from a rake of five-hole probes. Here, ten individual probes are mounted on a single probe shaft and used simultaneously. Use of this probe is made practical by the simplicity afforded by this algorithm.

NOMENCLATURE

a_{ij} = coefficients of the Taylor's series expansion of $C_{p_{avg}}$, Equation 5
 a_1, \dots, a_4 = coefficients of $\hat{C}_{p_{avg}}$, Equation 7
 \mathbf{a} = vector containing a_1, \dots, a_4 , Equation 13
 b_{ij} = coefficients of the Taylor's series expansion of C_{p_5} , Equation 6
 b_1, \dots, b_3 = coefficients of \hat{C}_{p_5} , Equation 8
 \mathbf{b} = vector containing b_1, \dots, b_3 , Equation 14
 $C_{p_{avg}}$ = probe average pressure coefficient, Equation 1
 $\hat{C}_{p_{avg}}$ = truncated Taylor's series approximation of $C_{p_{avg}}$, Equation 7
 C_{p_5} = probe center pressure coefficient, Equation 2
 \hat{C}_{p_5} = truncated Taylor's series approximation of C_{p_5} , Equation 8
 C_{p_v} = j direction pressure coefficient, Equation 3
 C_{p_w} = k direction pressure coefficient, Equation 4
 $C_{p_{max}}$ =

c_{ij}, d_{ij} = coefficients of the Taylor's series expansions of v and w , Equations 9 and 10
 c_1, \dots, c_6 = coefficients of \hat{v} and \hat{w} , Equations 11 and 12
 \mathbf{c} = vector containing c_1, \dots, c_6 , Equation 15
 $f_{p_{cal}}$ = influence function for $\sqrt{(\delta\hat{v})^2 + (\delta\hat{w})^2}$ resulting from δp_{cal}
 $f_{p_{exp}}$ = influence function for $\sqrt{(\delta\hat{v})^2 + (\delta\hat{w})^2}$ resulting from δp_{exp}
 f_φ = influence function for $\sqrt{(\delta\hat{v})^2 + (\delta\hat{w})^2}$ resulting from $\delta\varphi$
 $g_{p_{cal}}$ = influence function for δp_0 resulting from δp_{cal}
 $g_{p_{exp}}$ = influence function for δp_0 resulting from δp_{exp}
 $h_{p_{cal}}$ = influence function for δp resulting from δp_{cal}
 $h_{p_{exp}}$ = influence function for δp resulting from δp_{exp}
 \mathbf{m}_i = vector containing products of C_{p_v} and C_{p_w} . Used to determine \mathbf{a} in Equation 13
 \mathbf{n}_i = vector containing products of C_{p_v} and C_{p_w} . Used to determine \mathbf{b} in Equation 14
 \mathbf{o}_i = matrix containing products of C_{p_v} and C_{p_w} . Used to determine \mathbf{c} in Equation 15
 p = local static pressure
 p_0 = local total pressure
 p_i = pressure measured by the i th probe tube
 p_{avg} = average pressure measured by the four outer probe tubes, $p_{avg} = (p_1 + p_2 + p_3 + p_4)/4$
 r = rake probe radial position
 U, V, W = cartesian velocity vector components
 u, v, w = components of Cartesian unit vector in direction of velocity
 \hat{v}, \hat{w} = truncated Taylor's series approximations of v and w
 $\delta\hat{v}, \delta\hat{w}$ = flow direction result uncertainty
 v_0, w_0 = pitch and yaw offset, Equations 16 and 17
 v_1, w_1 = probe tip rotation parameters, Equation 18
 \mathbf{V} = cartesian velocity vector
 δp = static pressure result uncertainty
 δp_0 = total pressure result uncertainty
 δp_{exp} = experimental pressure measurand uncertainty
 δp_{cal} = calibration pressure measurand uncertainty
 $\delta\varphi$ = calibration flow direction measurand uncertainty
 θ = pitch angle

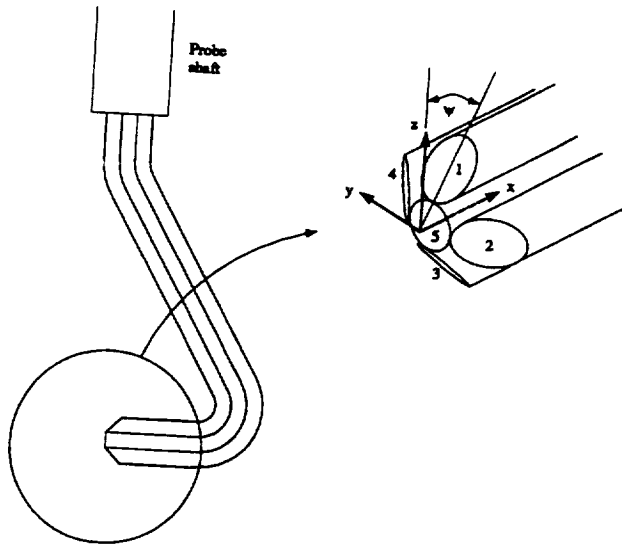


Figure 1 A typical five-hole probe

- ϕ = yaw angle
 ψ = probe outer tube opening angle
 ζ = rake probe circumferential position

INTRODUCTION

Figure 1 shows a typical five-hole probe and the coordinate system used in this analysis. The openings of the four outer tubes are inclined from the normal to their axes by angle ψ while the center tube opening is normal to its axis. The pressure sensed at the opening of each tube is denoted p_i . The subscript i refers to the probe opening, as defined in Figure 1. The mean velocity vector is $V = U i + V j + W k$ and the unit vector in the mean flow direction is $V/|V| = u i + v j + w k$. Table 1 prescribes the unit vectors in terms of pitch and yaw angles in both the pitch-yaw and yaw-pitch systems of angle definitions. The sign convention was chosen so that (small) positive values of pitch and yaw angle provide positive v and w velocity components. When flow angles are required in this analysis the pitch-yaw system is used however the conclusions are valid for the yaw-pitch system.

The ability to measure total and static pressure (hence velocity magnitude) and flow direction with a five-hole probe is well established. Two different measurement techniques have been employed. For the yaw-nulling method, the flow yaw angle is determined by the amount of rotation required until the pressures measured by tubes 2 and 4 are equal. Flow pitch angle is determined by the pressures of tubes 1, 3, and 5 and the results of

Unit vector	Pitch-yaw	Yaw-pitch
u	$\cos \theta \cos \phi$	$\cos \theta \cos \phi$
v	$\cos \theta \sin \phi$	$\sin \phi$
w	$\sin \theta$	$\sin \theta \cos \phi$

Table 1 Unit vectors

pitch angle calibration. For the non-nulling method, the probe remains stationary and calibration is used to determine flow direction.¹ In both methods, calibration is used to determine total and static pressure. Each method has advantages. Calibration and data reduction require less effort with the yaw-nulling method. When acquiring data in an experiment, the yaw-nulling method requires more time and more sophisticated actuation and data acquisition hardware than the non-nulling method. When the amount of data gathered in an experiment is large, the extra effort expended to calibrate the probe for the non-nulling method is more than compensated by the effort saved when acquiring data. This analysis is about the non-nulling method.

Four pressure coefficients, Equations 1–4, are used in the calibration and data reduction procedure. Over a range of Reynolds numbers and subsonic Mach numbers the four pressure coefficients depend on flow direction only. Calibration is used to determine the relationships that exist between the four pressure coefficients and flow direction. In data reduction, Cp_v and Cp_w allow flow direction to be determined, while Cp_s and Cp_{avg} allow total and static pressure to be determined.

$$Cp_{avg} = \frac{p_{avg} - p}{p_0 - p} \quad (1)$$

$$Cp_s = \frac{p_s - p}{p_0 - p} \quad (2)$$

$$Cp_v = \frac{p_2 - p_4}{p_5 - p_{avg}} \quad (3)$$

$$Cp_w = \frac{p_3 - p_1}{p_5 - p_{avg}} \quad (4)$$

There continues to be a great deal of interest regarding the need to quantify and report uncertainty in numerical and experimental fluid flow studies (Rood and Telionis, 1991 and Sutton, 1994). Most five-hole probe calibration and data reduction algorithms are not generally suited for an analytical treatment of uncertainty analysis. Uncertainty may be assessed by propagating measurand uncertainty through the data reduction programming by a numerical technique known as "jitter" analysis (Moffat, 1982). While the jitter technique allows the uncertainty of individual probes to be quantified, it provides little insight into basic processes underlying the uncertainty that analytical treatments yield. In the following section we develop an algorithm with a simplicity and accuracy that permits an analytical treatment of the propagation of uncertainty, revealing details about the relationships between probe geometry, calibration, data reduction and result uncertainty and providing guidance to improve measurement technique.

¹ The choice of pitch and yaw angle definitions depends on several factors. For the non-nulling technique the angle definition depends on the probe actuation hardware used in calibration. For the yaw-nulling technique the yaw-pitch angle definition must be used.

THE NEW ALGORITHM

The discussion up to this point is classical. Excellent descriptions are given by Bryer and Pankhurst (1971) and Treaster and Yocum (1979). Although other authors use different names and definitions, common to all these methods is the use of four pressure coefficients, two coefficients to determine flow direction and two coefficients to determine total and static pressure. Our algorithm differs from previous research in our choice of flow direction variables and how the relationships between the four coefficients and flow direction are formulated.

Traditionally, pitch and yaw angles are the variables used to express flow direction. Instead, we use components of the unit vector in the flow direction. Because the three components satisfy the criteria $u^2 + v^2 + w^2 = 1$, only two are required to uniquely specify flow direction (with the restriction that $u > 0$). We use v and w . Using two unit vector components instead of pitch and yaw angles has several advantages: 1) the calibration results do not depend on the choice of pitch-yaw or yaw-pitch angle definitions, 2) probe tip symmetry is expressed easier, 3) the relationships between pressure coefficients and flow direction are simpler and, 4) a step is removed from the data reduction procedure, where the desired answer is usually the velocity vector and not pitch and yaw angles. During calibration pitch and yaw angles are recorded and are later converted to unit vectors components according to the definitions in Table 1.

Two general classes of schemes that have been reported to express the relationships between the four pressure coefficients and flow direction are graphical methods (Dudzinski and Krause, 1969 and Bryer and Pankhurst, 1971) and interpolative methods involving spline fits of all the calibration data (Treaster and Yocum, 1979 and Lagrani *et al.*, 1989). Graphical methods are not suitable for large experimental data sets and the interpolative methods become cumbersome and slow when the amount of calibration data is large.

We use Taylor's series expansions in two variables, truncated to fifth order, to approximate the relationships between the four pressure coefficients and flow direction. What is unique in our approach is to identify and utilize the probe symmetry to reduce the number of required coefficients for all Taylor's series from sixty to thirteen. For data reduction, flow direction as well as total and static pressure are obtained from the probe data by direct calculation. No piecewise interpolative or iterative procedures are required.

An examination of Figure 1 will show that the five-hole probe possesses three types of geometric symmetry. They are: 1) symmetry with respect to reflection across the xz -plane, 2) symmetry with respect to reflection across the xy -plane, and 3) symmetry with respect to 90° rotation about the x -axis. The symmetry of the probe has important consequences for the relationships between the pressure coefficients and the flow direction variables. One result of symmetry is that within a range of flow directions about $v = 0$ and $w = 0$ there exists a one-to-one relationship between the flow direction variables v and w and the flow direction coefficients Cp_v and Cp_w . In fact, the ability to use a five-hole probe to measure flow direction requires the existence of this one-to-one relationship. This allows either v and w or Cp_v and Cp_w to be used as independent variables to express flow direction.

Since Cp_{avg} and Cp_5 depend on v and w , the one-to-one relationship described allows Cp_{avg} and Cp_5 to alternatively be considered functions of Cp_v and Cp_w . In Equations 5 and 6 the coefficients Cp_{avg} and Cp_5 are represented as a Taylor's series expansions in the variables Cp_v and Cp_w .²

$$Cp_{avg}(Cp_v, Cp_w) = \sum_{i=0}^{\infty} \sum_{j=0}^{\infty} a_{ij} Cp_v^i Cp_w^j \quad (5)$$

$$Cp_5(Cp_v, Cp_w) = \sum_{i=0}^{\infty} \sum_{j=0}^{\infty} b_{ij} Cp_v^i Cp_w^j \quad (6)$$

Symmetry relationships for Cp_{avg} and Cp_5 are listed below. Proofs of the results stated below are included in the Appendix:

$$\begin{aligned} Cp_{avg}(Cp_v, Cp_w) &= Cp_{avg}(-Cp_v, Cp_w) \\ Cp_{avg}(Cp_v, Cp_w) &= Cp_{avg}(Cp_v, -Cp_w) \\ Cp_{avg}(Cp_v, Cp_w) &= Cp_{avg}(Cp_w, -Cp_v) \\ Cp_5(Cp_v, Cp_w) &= Cp_5(-Cp_v, Cp_w) \\ Cp_5(Cp_v, Cp_w) &= Cp_5(Cp_v, -Cp_w) \\ Cp_5(Cp_v, Cp_w) &= Cp_5(Cp_w, -Cp_v) \end{aligned}$$

The symmetry conditions listed for the coefficients Cp_{avg} and Cp_5 greatly simplify their Taylor's series representation. Also, subsonic flow aerodynamics requires $Cp_5(0, 0)$ equal one. In the Appendix, the following results for the Taylor's series are derived:

$$\begin{aligned} a_{ij} &= 0, \quad j = 1, 3, 5, \dots \\ a_{ij} &= 0, \quad i = 1, 3, 5, \dots \\ a_{ij} &= a_{ji} \\ b_{ij} &= 0, \quad j = 1, 3, 5, \dots \\ b_{ij} &= 0, \quad i = 1, 3, 5, \dots \\ b_{ij} &= b_{ji} \end{aligned}$$

The simplified Taylor's series for Cp_{avg} and Cp_5 , truncated at fifth order and given by Equations 7 and 8, result in seven undetermined series coefficients, rather than thirty that would generally be required. The Taylor's series coefficients have been renumbered in Equations 7 and 8 for clarity. The "hat" symbol that appears above the pressure coefficient is used to distinguish the Taylor's series approximation from the pressure coefficient based on actual measurement.

$$\begin{aligned} \hat{Cp}_{avg} &= a_1 + \\ & a_2(Cp_v^2 + Cp_w^2) + \\ & a_3(Cp_v^4 + Cp_w^4) + a_4 Cp_v^2 Cp_w^2 \end{aligned} \quad (7)$$

$$\begin{aligned} \hat{Cp}_5 &= 1 + \\ & b_1(Cp_v^2 + Cp_w^2) + \\ & b_2(Cp_v^4 + Cp_w^4) + b_3 Cp_v^2 Cp_w^2 \end{aligned} \quad (8)$$

² Using Cp_v and Cp_w as independent variables in Equations 5 and 6 allows Cp_{avg} and Cp_5 to be calculated directly from Cp_v and Cp_w . If v and w had been used as independent variables in Equation 5 and 6, then an additional step would be required in data reduction when determining Cp_{avg} and Cp_5 .

For flow direction, the unit vector components v and w are represented in Equations 9 and 10 by Taylor's series expansions in the variables Cp_v and Cp_w .³

$$v(Cp_v, Cp_w) = \sum_{i=0}^{\infty} \sum_{j=0}^{\infty} c_{ij} Cp_v^i Cp_w^j \quad (9)$$

$$w(Cp_v, Cp_w) = \sum_{i=0}^{\infty} \sum_{j=0}^{\infty} d_{ij} Cp_v^i Cp_w^j \quad (10)$$

In the Appendix the following probe symmetry results for v and w as functions of Cp_v and Cp_w are derived.

$$\begin{aligned} v(Cp_v, Cp_w) &= -v(-Cp_v, Cp_w) \\ v(Cp_v, Cp_w) &= v(Cp_v, -Cp_w) \\ w(Cp_v, Cp_w) &= w(-Cp_v, Cp_w) \\ w(Cp_v, Cp_w) &= -w(Cp_v, -Cp_w) \\ v(Cp_v, Cp_w) &= w(Cp_w, -Cp_v) \end{aligned}$$

In the same manner used for Cp_{avg} and Cp_5 , the results listed above greatly simplify the Taylor's series representation of v and w . In the Appendix, the following results for the Taylor's series coefficients are derived.

$$\begin{aligned} c_{ij} &= 0, \quad i = 0, 2, 4, \dots \\ c_{ij} &= 0, \quad j = 1, 3, 5, \dots \\ d_{ij} &= 0, \quad i = 1, 3, 5, \dots \\ d_{ij} &= 0, \quad j = 0, 2, 4, \dots \\ c_{ij} &= d_{ji} \end{aligned}$$

Equations 11 and 12 give the Taylor's series approximation of v and w truncated at fifth order. The series coefficients have been renumbered in Equations 11 and 12 for clarity. The same series coefficients appear in both Taylor's series expansions. Rather than requiring thirty coefficients, the truncated Taylor's series only requires six. The "hat" symbol again is used to distinguish Taylor's series approximations from actual values.

$$\begin{aligned} \hat{v}(Cp_v, Cp_w) &= c_1 Cp_v + \\ & c_2 Cp_v^3 + c_3 Cp_v Cp_w^2 + \\ & c_4 Cp_v^5 + c_5 Cp_v^3 Cp_w^2 + c_6 Cp_v Cp_w^4 \end{aligned} \quad (11)$$

$$\begin{aligned} \hat{w}(Cp_v, Cp_w) &= c_1 Cp_w + \\ & c_3 Cp_v^2 Cp_w + c_2 Cp_v^3 + \\ & c_6 Cp_v^4 Cp_w + c_5 Cp_v^2 Cp_w^3 + c_4 Cp_v^5 \end{aligned} \quad (12)$$

Note that all the desired simplified Taylor's series, given by Equations 7, 8, 11, and 12 include terms involving products of Cp_v and Cp_w . In order to evaluate these coefficients requires taking calibration data over a range of both pitch and yaw angle

³ Note that v and w are dependent variables in Equations 9 and 10. In data reduction, this allows v and w to be calculated directly from measured values of Cp_v and Cp_w . If Cp_v and Cp_w were expressed as functions of v and w , then a numerical solution scheme would be required to calculate values of v and w from measured values of Cp_v and Cp_w .

values. In other words, it is not sufficient to simply vary pitch while yaw equals zero and *vice-versa*.

The coefficients themselves are found by a least-squares procedure. This results in three systems of simultaneous linear equations, the solutions of which are the Taylor's series coefficients. The three systems of equations are given in Equations 13, 14 and 15. The summation in these equations is over all data acquired during calibration. These equations are solved directly by matrix inversion.

$$\sum_i m_i Cp_{avg,i} = \sum_i (m_i m_i^T) a$$

$$m_i = \begin{bmatrix} 1 \\ Cp_{v,i}^2 + Cp_{w,i}^2 \\ Cp_{v,i}^4 + Cp_{w,i}^4 \\ Cp_{v,i}^2 Cp_{w,i}^2 \end{bmatrix} \quad a = \begin{bmatrix} a_1 \\ a_2 \\ a_3 \\ a_4 \end{bmatrix} \quad (13)$$

$$\sum_i n_i (Cp_{5,i} - 1) = \sum_i (n_i n_i^T) b$$

$$n_i = \begin{bmatrix} Cp_{v,i}^2 + Cp_{w,i}^2 \\ Cp_{v,i}^4 + Cp_{w,i}^4 \\ Cp_{v,i}^2 Cp_{w,i}^2 \end{bmatrix} \quad b = \begin{bmatrix} b_1 \\ b_2 \\ b_3 \end{bmatrix} \quad (14)$$

$$\sum_i o_i \begin{bmatrix} v_i \\ w_i \end{bmatrix} = \sum_i (o_i o_i^T) c$$

$$o_i = \begin{bmatrix} Cp_{v,i} & Cp_{w,i} \\ Cp_{v,i}^3 & Cp_{w,i}^3 \\ Cp_{v,i} Cp_{w,i}^2 & Cp_{v,i}^2 Cp_{w,i} \\ Cp_{v,i}^5 & Cp_{w,i}^5 \\ Cp_{v,i}^3 Cp_{w,i}^2 & Cp_{v,i}^2 Cp_{w,i}^3 \\ Cp_{v,i} Cp_{w,i}^4 & Cp_{v,i}^4 Cp_{w,i} \end{bmatrix} \quad c = \begin{bmatrix} c_1 \\ c_2 \\ c_3 \\ c_4 \\ c_5 \\ c_6 \end{bmatrix} \quad (15)$$

There are several additional details included in the calibration and data reduction algorithm. Figure 1 shows a Cartesian coordinate system relative to the probe tip. It is useful to think of a second Cartesian coordinate system relative to the probe shaft. The probe shaft coordinate system has its z -axis parallel to the probe shaft and its x -axis is the datum used for measuring probe shaft rotation. In practice, all measurements of the probe orientation are relative to the probe shaft coordinate system. Ideally, the probe tip is mounted so that the two coordinate systems have identical orientations. In reality this is highly unlikely. Four parameters are needed to account for misalignment between the probe tip and probe shaft. They are pitch and yaw offset and two tip rotation parameters.

Pitch and yaw offset relate the difference between the x -axes of both coordinate systems. The value of pitch offset is determined by the probe geometry and should not change unless the probe is damaged. The yaw offset value is established whenever the probe is attached to the calibration rig or experimental rig. Thus, the yaw offset may change whenever the probe is moved.

The tip rotation parameters relate the difference between the y - and z -axes of both coordinate systems when the x -axis difference has been eliminated. This is shown in Figure 2. To be rigorously correct, if the two tip rotation parameters are such that $v_1 \neq w_1$, then the probe tip is skewed and the symmetry criterion that were used to develop the calibration procedure are not satisfied.

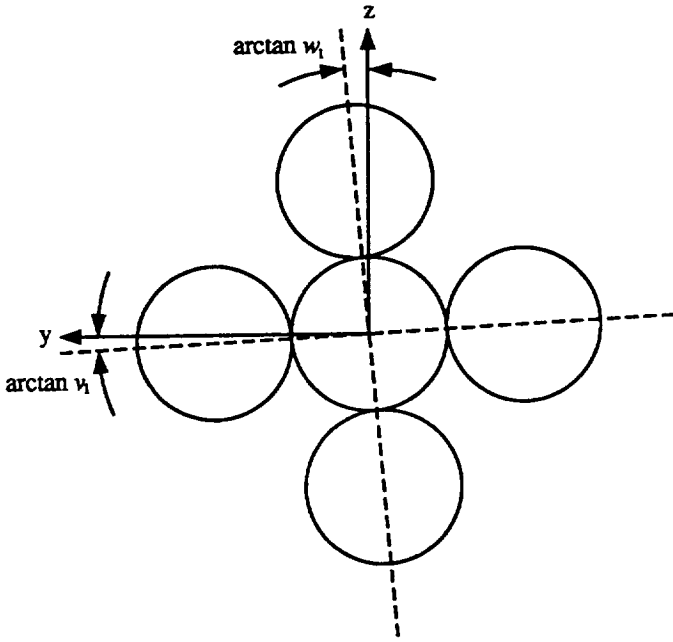


Figure 2 Probe tip rotation angles

However, small amounts of skewness, which are unavoidable, result in only a small deviation from the symmetry criterion. Measuring and allowing for minor skewness in this manner can be viewed as a perturbation of the symmetry condition. The two tip rotation angles are also determined by the probe geometry and are unlikely to change unless the probe is damaged.

Values of the four parameters are determined from calibration data. This is necessary because it is impractical to accurately determine these quantities from observations of the probe geometry alone. First, pitch and yaw angles recorded during calibration are converted to unit vector components. The pitch offset is determined by evaluating the data recorded for zero yaw angle (hence $v = 0$) to find the value of w when $Cp_w = 0$. This value, w_0 , is the pitch offset. A least square error procedure is used to determine its numerical value. Likewise, the yaw offset is determined by evaluating the data recorded for zero pitch angle (hence $w = 0$) to find the value of v when $Cp_v = 0$. Equations 16 and 17 transform unit vector components for pitch offset (Equation 16) and yaw offset (Equation 17). The primed unit vector components indicate values uncorrected for offset.

$$\begin{bmatrix} u \\ v \\ w \end{bmatrix} = \begin{bmatrix} \sqrt{1-w_0^2} & 0 & w_0 \\ 0 & 1 & 0 \\ -w_0 & 0 & \sqrt{1-w_0^2} \end{bmatrix} \begin{bmatrix} u' \\ v' \\ w' \end{bmatrix} \quad (16)$$

$$\begin{bmatrix} u \\ v \\ w \end{bmatrix} = \begin{bmatrix} \sqrt{1-v_0^2} & v_0 & 0 \\ -v_0 & \sqrt{1-v_0^2} & 0 \\ 0 & 0 & 1 \end{bmatrix} \begin{bmatrix} u' \\ v' \\ w' \end{bmatrix} \quad (17)$$

Determining the tip rotation angles is slightly more complicated. If there were no tip rotation, then the vector $\nabla Cp_v(0,0)$ would point in the direction of the y -axis and the vector $\nabla Cp_w(0,0)$ would point in the direction of the z -axis. The tip rotation

parameters are a measure of the angles between the two gradient vectors and their corresponding axes. They are calculated using Equation 18. Values of the partial derivatives are determined with another least squares procedure. Equation 19 is the final relationship applied to transform unit vector components from the probe shaft coordinate system to the probe tip coordinate system. The primed unit vector components indicate values uncorrected for tip rotation.

$$\begin{aligned} v_1 &= \frac{\frac{\partial Cp_v}{\partial v}(0,0)}{\frac{\partial Cp_w}{\partial w}(0,0)} \\ w_1 &= \frac{\frac{\partial Cp_w}{\partial v}(0,0)}{\frac{\partial Cp_w}{\partial w}(0,0)} \end{aligned} \quad (18)$$

$$\begin{bmatrix} u \\ v \\ w \end{bmatrix} = \frac{\begin{bmatrix} 1 & 0 & 0 \\ 0 & \frac{1}{\sqrt{1+w_1^2}} & -\frac{v_1}{\sqrt{1+v_1^2}} \\ 0 & \frac{w_1}{\sqrt{1+w_1^2}} & \frac{1}{\sqrt{1+v_1^2}} \end{bmatrix} \begin{bmatrix} u' \\ v' \\ w' \end{bmatrix}}{\left(\frac{1+v_1 w_1}{\sqrt{(1+v_1^2)(1+w_1^2)}} \right)^{1/3}} \quad (19)$$

In summary, the steps used in the probe calibration algorithm are:

1. Express the measured pressures as pressure coefficients Cp_{avg} , Cp_s , Cp_v and Cp_w using Equations 1, 2, 3 and 4.
2. Convert the pitch and yaw angles recorded during calibration to unit vector components using the definitions from Table 1.
3. Determine pitch and yaw offset w_0 and v_0 from the calibration data and apply them to the unit vector component values using Equations 16 and 17.
4. Determine the tip rotations parameters v_1 and w_1 from the calibration data using Equation 18 and apply them to the unit vector component values using Equation 19.
5. Calculate the $\hat{Cp}_{avg}(Cp_v, Cp_w)$ Taylor's series coefficients using Equation 13.
6. Calculate the $\hat{Cp}_s(Cp_v, Cp_w)$ Taylor's series coefficients using Equation 14.
7. Calculate the $\hat{v}(Cp_v, Cp_w)$ and $\hat{w}(Cp_v, Cp_w)$ Taylor's series coefficients using Equation 15.

Once the probe is calibrated, the procedure for reducing experimental data is straightforward. The steps that are applied are listed below:

1. Determine the coefficients Cp_v and Cp_w from the probe pressure data using Equations 3 and 4.
2. Substitute the values of Cp_v and Cp_w into Equations 11 and 12 to calculate \hat{v} and \hat{w} .
3. Substitute the values of Cp_v and Cp_w into Equations 7 and 8 to calculate \hat{Cp}_{avg} and \hat{Cp}_s .
4. Calculate total and static pressure with Equation 20, which is simply a rearrangement of Equations 1 and 2 (with \hat{Cp}_{avg} and \hat{Cp}_s substituted for Cp_{avg} and Cp_s).

$$\begin{bmatrix} p_0 \\ p \end{bmatrix} = \frac{\begin{bmatrix} 1 - \hat{Cp}_{avg} & \hat{Cp}_s - 1 \\ -\hat{Cp}_{avg} & \hat{Cp}_s \end{bmatrix} \begin{bmatrix} p_s \\ p_{avg} \end{bmatrix}}{\hat{Cp}_s - \hat{Cp}_{avg}} \quad (20)$$

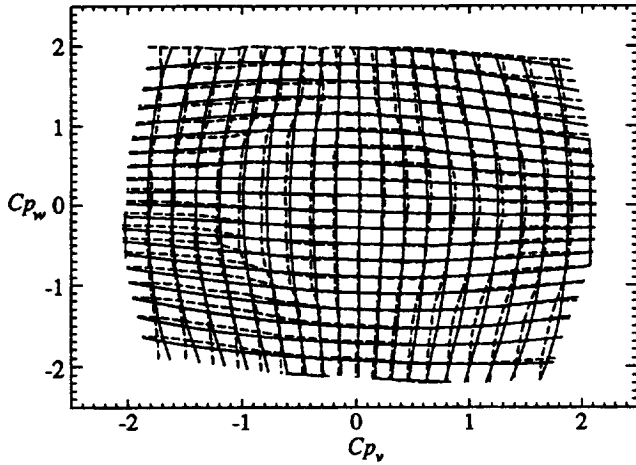


Figure 3 Pitch and yaw calibration results

5. Convert the unit vector components from the probe tip coordinate system to the probe shaft coordinate system using, in order, Equations 21, 22 and 23. These equations are the inverse of Equations 19, 17 and 16.

$$\begin{bmatrix} u' \\ v' \\ w' \end{bmatrix} = \frac{\begin{bmatrix} 1 & 0 & 0 \\ 0 & \frac{1}{\sqrt{1+v_1^2}} & \frac{v_1}{\sqrt{1+v_1^2}} \\ 0 & -\frac{w_1}{\sqrt{1+w_1^2}} & \frac{1}{\sqrt{1+w_1^2}} \end{bmatrix} \begin{bmatrix} u \\ v \\ w \end{bmatrix}}{\left(\frac{1+v_1 w_1}{\sqrt{(1+v_1^2)(1+w_1^2)}} \right)^{1/3}} \quad (21)$$

$$\begin{bmatrix} u' \\ v' \\ w' \end{bmatrix} = \begin{bmatrix} \sqrt{1-v_0^2} & v_0 & 0 \\ -v_0 & \sqrt{1-v_0^2} & 0 \\ 0 & 0 & 1 \end{bmatrix} \begin{bmatrix} u \\ v \\ w \end{bmatrix} \quad (22)$$

$$\begin{bmatrix} u' \\ v' \\ w' \end{bmatrix} = \begin{bmatrix} \sqrt{1-w_0^2} & 0 & -w_0 \\ 0 & 1 & 0 \\ w_0 & 0 & \sqrt{1-w_0^2} \end{bmatrix} \begin{bmatrix} u \\ v \\ w \end{bmatrix} \quad (23)$$

It is worth reiterating the fact that neither the calibration or data reduction procedures requires iteration. All results are obtained by direct calculation.

Experimental Verification of the Algorithm

It remains to show that the simplified Taylor's series, given by Equations 7, 8, 11 and 12, whose derivation was based on the symmetry of an ideal probe, can faithfully represent the calibration data of an actual five-hole probe. Flow direction calibration results for a typical probe is shown in Figure 3. Calibration data were obtained for pitch and yaw angles ranging from -20° to $+20^\circ$ in 2° increments. The Mach number of the calibration airstream was approximately 0.4. The independent variables of Figure 3 are the coefficients Cp_v and Cp_w . Plotted together are contour levels of the unit vector components v and w . Solid lines are the Taylor's series approximations, broken lines are calibration data. The lines of constant v appear nominally vertical and lines of

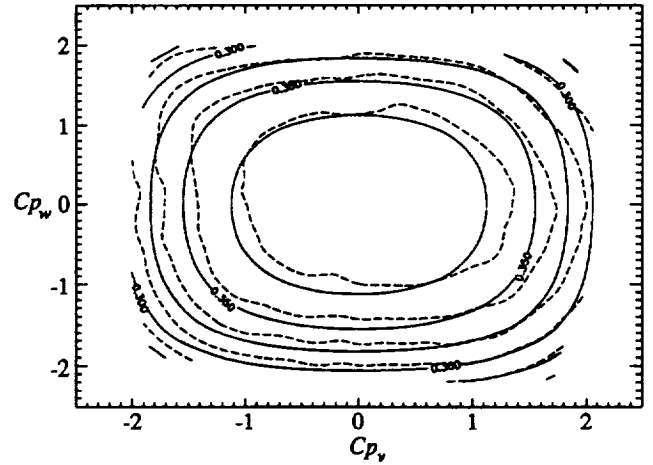


Figure 4 Cp_{avg} calibration results

constant w nominally horizontal. An examination of Figure 3 will verify the validity of Equations 11 and 12. Average (RMS) error for both v and w is less than 0.0053 (or less than 0.3°). Likewise, contour plots of the Cp_{avg} and Cp_s coefficients as functions of independent variables Cp_v and Cp_w are shown in Figures 4 and 5. Solid lines are the Taylor's series approximations, broken lines are calibration data. Average error for both coefficients is less than 1% of dynamic pressure. Again, the agreement is quite good.

Probe Geometry and Response

By making some plausible assumptions it is possible to relate the leading order probe calibration coefficients for \hat{Cp}_{avg} , \hat{v} and \hat{w} to probe geometry. The leading order term for \hat{Cp}_s was determined earlier from aerodynamic considerations, that is $\hat{Cp}_s(0,0) = 1$. This analysis leads to the following results; $a_1 \approx \cos^2 \psi$ and $c_1 \approx \frac{1}{4} \sin \psi$. These results are approximate and are not intended to replace calibration, but they do provide some insight into the effect of probe geometry on probe response and uncertainty.

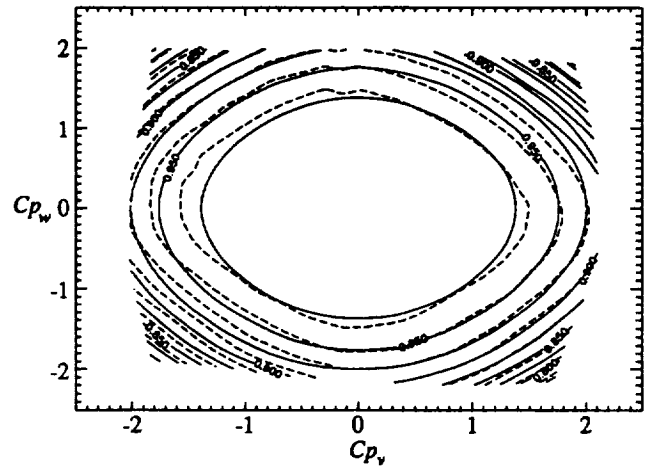


Figure 5 Cp_s calibration results

Restrictions For Large Flow Angles

As flow angles increase eventually this and similar algorithms become unreliable. There are several mathematical reasons that will cause the algorithm to fail. The first is when the relationship between the flow direction variables v and w and the flow direction coefficients Cp_v and Cp_w is no longer one-to-one. This relationship is truly one-to-one only if we restrict the set of flow direction variables and corresponding flow direction coefficients to within a neighborhood of $Cp_v = 0$ and $Cp_w = 0$ that satisfies Equation 24. Where Equation 24 is not satisfied can be estimated if we restrict the pressure coefficients such that $Cp_v = Cp_w = Cp_{max}$ which will lead to two degenerate fourth order equations, Equations 25 and 26. The roots of Equations 25 and 26 are determined using the quadratic equation.

$$\det \begin{bmatrix} \frac{\partial v}{\partial Cp_v} & \frac{\partial v}{\partial Cp_w} \\ \frac{\partial w}{\partial Cp_v} & \frac{\partial w}{\partial Cp_w} \end{bmatrix} \neq 0 \quad (24)$$

$$(5c_4 + c_5 - 3c_6)Cp_{max}^4 + (3c_2 - c_3)Cp_{max}^2 + c_1 = 0 \quad (25)$$

$$5(c_4 + c_5 + c_6)Cp_{max}^4 + 3(c_2 + c_3)Cp_{max}^2 + c_1 = 0 \quad (26)$$

A second reason for the algorithm to fail is when the relationship between probe pressures p_s and p_{avg} and total and static pressure p_0 and p is no longer one-to-one. This restricts the set of flow direction variables and corresponding flow direction coefficients to a domain containing $Cp_v = 0$ and $Cp_w = 0$ that satisfies Equation 27. Where Equation 27 is not satisfied is estimated by the same restriction, $Cp_v = Cp_w = Cp_{max}$, which leads to another degenerate fourth order equation, Equation 28.

$$\det \begin{bmatrix} \frac{\partial p_s}{\partial p_0} & \frac{\partial p_s}{\partial p} \\ \frac{\partial p_{avg}}{\partial p_0} & \frac{\partial p_{avg}}{\partial p} \end{bmatrix} = (Cp_s - Cp_{avg})^2 \neq 0 \quad (27)$$

$$(2(b_2 - a_3) + (b_3 - a_4))Cp_{max}^4 + 2(b_1 - a_2)Cp_{max}^2 + 1 - a_1 = 0 \quad (28)$$

All roots of Equations 25, 26 and 28 are examined and the smallest positive root is substituted into Equation 29. With the flow direction variables restricted to a domain satisfying Equation 29 both the relationship between the flow direction variables and the flow direction coefficients is one-to-one and the relationship between probe pressures p_s and p_{avg} and total and static pressure is one-to-one and the algorithm will yield meaningful results. For the five-hole probe calibration results presented in Figures 3–5, the restricted domain is approximately $v^2 + w^2 < 0.25$ or flow angles approximately less than 30° . The size of the restricted domain for this example is being limited by Equation 24.

$$v^2 + w^2 < 2(c_1 Cp_{max} + (c_2 + c_3)Cp_{max}^3 + (c_4 + c_5 + c_6)Cp_{max}^5) \quad (29)$$

UNCERTAINTY ANALYSIS

Because of the new algorithm's simplicity and accuracy, it is well-suited to an analytical treatment (as opposed to a "jitter" or numerical technique) of the propagation of uncertainty in five-hole probe measurement. The objective of the uncertainty analysis is to quantify uncertainty of five-hole probe measurement results (e.g., total pressure, static pressure, and flow direction) and determine the dependence of the measurement uncertainty on the uncertainty of all underlying experimental and calibration measurements. These results will provide a general procedure that other researchers may use to determine five-hole probe measurement uncertainty and provide guidance to improve five-hole probe measurement technique by pinpointing greatest sources of uncertainty.

To discuss uncertainty, we have adopted the terminology of Kline (1985), where *measurand* describes a physical quantity that is measured and *result* describes a quantity that is obtained from a calculation involving measurands. Mathematically, results are dependent variables and measurands are independent variables. Equation 30 shows the dependence of the uncertainty of the result δR upon the uncertainty of the n measurands $\delta x_1, \dots, \delta x_n$. In our case the results are total pressure, static pressure, and the two unit vector components v and w (collectively referred to as flow direction).

$$(\delta R)^2 = \left(\frac{\partial R}{\partial x_1} \delta x_1 \right)^2 + \dots + \left(\frac{\partial R}{\partial x_n} \delta x_n \right)^2 \quad (30)$$

The uncertainty of the flow direction results calculated in data reduction ultimately depend on the uncertainty of the five values of probe pressure measured in the experiment (referred to as experimental pressure measurands) and the uncertainty of *each* measurement of the five probe pressures and flow angles acquired in probe calibration (referred to as calibration pressure measurands and calibration flow direction measurands). The dependence of flow direction results upon all intermediate steps of data reduction is illustrated in Figure 6. The darker paths represent values or results that depend wholly on experimental data and lighter paths values or results that depend wholly on calibration data. The uncertainty of flow direction results are determined from repeated use of Equation 30. For instance, $\delta \hat{v}$ and $\delta \hat{w}$ depend on δCp_v , δCp_w , and $\delta c_1, \dots, \delta c_6$. The uncertainty δCp_v depends on $\delta p_2, \delta p_4, \delta p_5$ and δp_{avg} and so on. This procedure is repeated until all the dependence shown in Figure 6 is accounted for.

Consider the common situation when either a single pressure transducer is used to measure all pressures or several equivalent pressure transducers are used. Then, their individual uncertainties will be equal. That is, allowing for the possibility that the transducer(s) used for calibration and experiment are different, for calibration $\delta p_{1,k} = \dots = \delta p_{5,k} = \delta p_{cal}$ for all k , and for experiment $\delta p_1 = \dots = \delta p_5 = \delta p_{exp}$. Likewise, if the same instrument is used to measure pitch and yaw angles to determine flow direction throughout calibration then their individual uncertainties are equal, in which case $\delta \theta_k = \delta \phi_k = \delta \varphi$. With these conditions the uncertainty of the flow direction result depends on the product of three measurand uncertainty parameters; $\delta p_{exp}/(p_0 - p)$, $\delta p_{cal}/(p_0 - p)$ and $\delta \varphi$, with their influence functions; $f_{p_{exp}}$, $f_{p_{cal}}$ and f_{φ} , according to the relationship given by

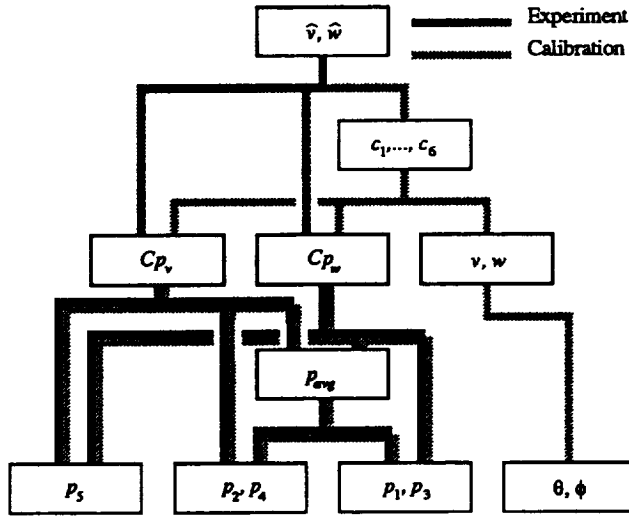


Figure 6 Propagation of uncertainty in flow direction results

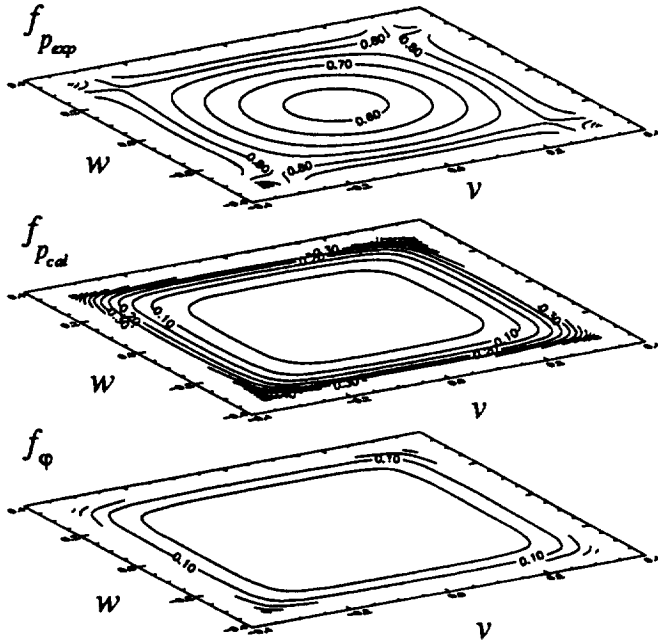


Figure 7 Uncertainty in flow direction results

Equation 31. Note that both measurand pressure uncertainties have been nondimensionalized with dynamic pressure. In Equation 31 uncertainties for both flow direction results have been combined to give an overall measure of flow direction result uncertainty.

$$(\delta \hat{v})^2 + (\delta \hat{w})^2 = f_{p_{exp}}^2 \left(\frac{\delta p_{exp}}{p_0 - p} \right)^2 + f_{p_{cal}}^2 \left(\frac{\delta p_{cal}}{p_0 - p} \right)^2 + f_{\varphi}^2 (\delta \varphi)^2 \quad (31)$$

The three measurand uncertainty influence functions in Equation 31 are functions of flow direction. Plotted in Figure 7 are

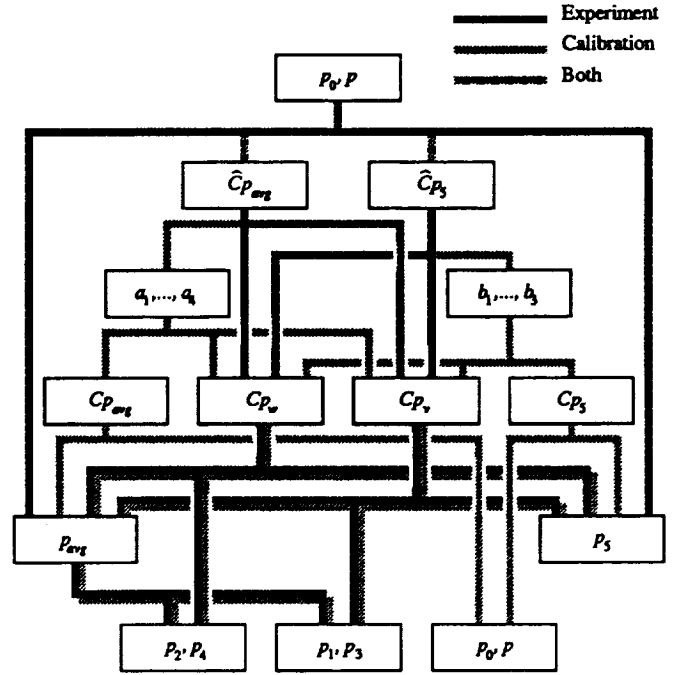


Figure 8 Propagation of error in total and static pressure results

contour levels of the influence functions. The data used to validate the calibration and reduction algorithm were used to evaluate the influence functions. The contour plots of the influence functions are over the range of flow direction used when calibrating the probe, that is pitch and yaw angles varying from -20° to $+20^\circ$. Several conclusions may be drawn from Figure 7. The value of both influence functions $f_{p_{cal}}$ and f_{φ} are zero when $v = 0$ and $w = 0$. This is not true for $f_{p_{exp}}$, however, which has the value $f_{p_{exp}}(0, 0) = 2c_1/(1 - a_1)$. This is a general observation that is valid for all five-hole probes calibrated with this algorithm. In practical terms this means that for modest flow angles, most or all flow direction result uncertainty comes from uncertainty in the experimental pressure measurands. For large flow angles, near the boundary of the calibration domain, the values of f_{φ} and particularly $f_{p_{cal}}$ grow rapidly. However, levels of $f_{p_{cal}}$ and f_{φ} generally are less than $f_{p_{exp}}$ except for large values of both v and w where $f_{p_{exp}}$ actually decreases.

Like flow direction, the uncertainty of total and static pressure results calculated in data reduction depend on the uncertainty of the five values of probe pressure measured in the experiment, the uncertainty of each measurement of the five probe pressures acquired in probe calibration as well as each measurement of the calibration stream's total and static pressure. Figure 8 shows the dependence of total and static pressure results on intermediate data reduction results. Because flow direction does not appear in Figure 8 the uncertainty of total and static pressure results do not explicitly depend on calibration flow direction measurand uncertainty. Values of total and static pressure result uncertainties are determined by repeated use of Equation 30.

Figure 9 shows contour levels of the two measurand uncertainty influence functions for total pressure in Equation 32. There are

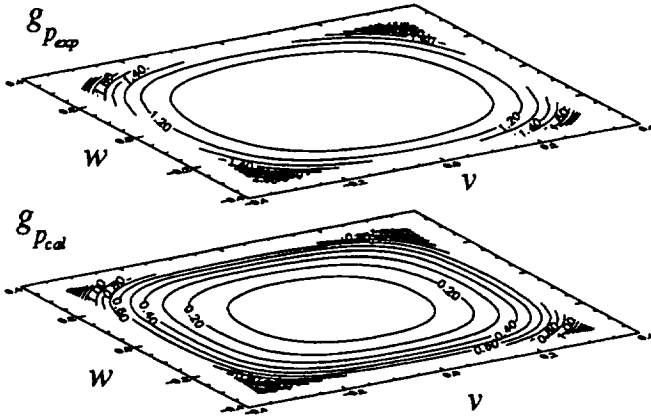


Figure 9 Uncertainty in total pressure results

several similarities between the total pressure result uncertainty influence functions and the corresponding flow direction result uncertainty influence functions shown in Figure 7. First, the value of $g_{p_{cal}}$ is zero when $v = 0$ and $w = 0$ while $g_{p_{exp}}(0, 0)$ is nonzero. Like flow direction result uncertainty, for small flow angles the total pressure result uncertainty comes almost entirely from uncertainty in the experimental pressure measurands. In fact, $g_{p_{exp}}(0, 0) = 1$ which simply means that it is impossible for total pressure result uncertainty to be less than experimental pressure measurand uncertainty. The value of $g_{p_{cal}}$ increases quickly away from the origin, however, values of $g_{p_{cal}}$ remain less than $g_{p_{exp}}$.

$$\left(\frac{\delta p_0}{p_0 - p}\right)^2 = g_{p_{exp}}^2 \left(\frac{\delta p_{exp}}{p_0 - p}\right)^2 + g_{p_{cal}}^2 \left(\frac{\delta p_{cal}}{p_0 - p}\right)^2 \quad (32)$$

Figure 10 shows contour levels of the two measurand uncertainty influence functions for static pressure result uncertainty in Equation 33. There are several interesting differences with the corresponding influence functions for flow direction result uncertainty and total pressure result uncertainty. First, the value of $h_{p_{cal}}$ is nonzero when $v = 0$ and $w = 0$, while $h_{p_{exp}}(0, 0) = 1$. This means that for small flow angles, the uncertainty of static pressure results are necessarily greater than the uncertainty of total pressure results. This fact confirms the belief that static pressure determined by a five-hole probe is not as "accurate" as total pressure obtained with the same probe.

$$\left(\frac{\delta p}{p_0 - p}\right)^2 = h_{p_{exp}}^2 \left(\frac{\delta p_{exp}}{p_0 - p}\right)^2 + h_{p_{cal}}^2 \left(\frac{\delta p_{cal}}{p_0 - p}\right)^2 \quad (33)$$

The preceding analysis can be used to provide guidance in ways to reduce five-hole probe result uncertainty. In general, reducing result uncertainty can be achieved by either reducing the measurand uncertainty parameters $\delta p_{exp}/(p_0 - p)$, $\delta p_{cal}/(p_0 - p)$ and $\delta \varphi$ or by reducing their respective influence functions. The measurand uncertainty parameters $\delta p_{exp}/(p_0 - p)$ and $\delta p_{cal}/(p_0 - p)$ can be reduced by either decreasing the numerator by using more accurate transducers or by averaging repeated measurements, or

by increasing the denominator by raising the dynamic pressure of the flow. However, the ability to increase dynamic pressure is limited since this typically requires higher velocities and as the sonic velocity is approached compressibility effects become significant. The measurand uncertainty parameter $\delta \varphi$ can also be reduced by using a more accurate angle measuring device or averaging repeated measurements.

The measurand uncertainty influence functions $f_{p_{exp}}$, $g_{p_{exp}}$, and $h_{p_{exp}}$ depend on the probe calibration coefficients as well as v and w . To reduce $f_{p_{exp}}$, $g_{p_{exp}}$ and $h_{p_{exp}}$ requires changes in the probe calibration coefficients, which are determined by the probe geometry. To reduce $f_{p_{exp}}$, $g_{p_{exp}}$ and $h_{p_{exp}}$ requires making physical modifications to the probe. For flow direction uncertainty, $f_{p_{exp}}(0, 0) = 2c_1/(1 - a_1)$. Using the approximations stated earlier relating probe calibration coefficients to probe geometry yields the approximation $f_{p_{exp}}(0, 0) \approx 0.5/\sin \psi$. Therefore, flow direction result uncertainty can be improved by increasing the angle of the openings of the four outer tubes. However, intuition says that this will also restrict the range of flow angles for which the probe can be used. For total and static pressure result uncertainty $g_{p_{exp}}(0, 0) = h_{p_{exp}}(0, 0) = 1$. This observation is valid for all five-hole probes, so it is not possible to lower this value by making modifications to the probe. Modifying the probe will not improve total or static pressure result uncertainty for small flow angles.

The measurand uncertainty influence functions $f_{p_{cal}}$, $g_{p_{cal}}$, $h_{p_{cal}}$ and f_φ depend on calibration data as well as v and w . The probe calibration coefficients themselves do not explicitly appear in $f_{p_{cal}}$, $g_{p_{cal}}$, $h_{p_{cal}}$, and f_φ , however modifications to the probe geometry will effect them by changing the calibration measurements. The influence functions $f_{p_{cal}}$, $g_{p_{cal}}$, $h_{p_{cal}}$, and f_φ may be reduced by modifying the probe calibration procedure. One way of accomplishing this is by acquiring more calibration data. For n total calibration measurements used the influence functions $f_{p_{cal}}$, $g_{p_{cal}}$, $h_{p_{cal}}$, and f_φ are approximately $O(1/\sqrt{n})$ so the overall levels of $f_{p_{cal}}$, $g_{p_{cal}}$, $h_{p_{cal}}$ and f_φ may be approximately halved by acquiring four times as much calibration data. To verify this the uncertainty values presented earlier were compared to uncertainty values calculated using a subset of the original calibration data containing one-fourth of the number of calibration

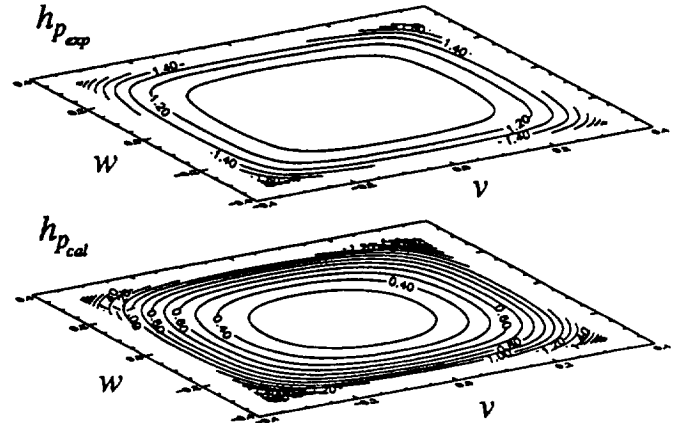


Figure 10 Uncertainty in static pressure results

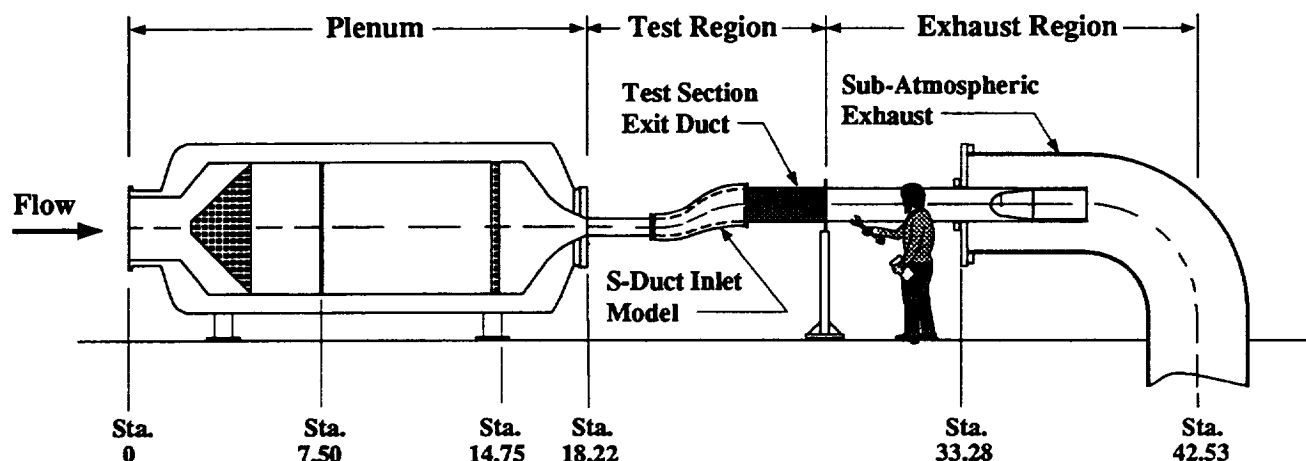


Figure 11 The Internal Fluid Mechanics Facility (IFMF) (Dimensions in feet)

data. This subset was obtained by skipping alternating rows of pitch and yaw data so that the distribution of pitch and yaw angles for the calibration data subset was equivalent to the original calibration data set. This analysis showed that the overall values of the influence functions $f_{p_{cal}}$, $g_{p_{cal}}$, $h_{p_{cal}}$ and f_{φ} were nominally greater by a factor of two for the smaller calibration data set. The influence functions $f_{p_{exp}}$, $g_{p_{exp}}$ and $h_{p_{exp}}$ were unchanged, as was expected.

Changing the distribution of pitch and yaw values used for calibration will also change $f_{p_{cal}}$, $g_{p_{cal}}$, $h_{p_{cal}}$, and f_{φ} . In general, these influence functions are reduced when the pitch and yaw values used for calibration are concentrated at higher flow angles. This was confirmed by using two subsets of the original calibration data. Both subsets contained the same amount of data, but one subset used calibration data acquired at large flow angles while the other used data acquired at small flow angles. The resulting values of $f_{p_{cal}}$, $g_{p_{cal}}$, $h_{p_{cal}}$, and f_{φ} were compared and showed interesting results. For total pressure result uncertainty, the value of $g_{p_{cal}}$ at large flow angles from the large flow angle calibration data was significantly less (by a factor of four) than the corresponding small flow angle calibration data set, while $g_{p_{cal}}(0,0) = 0$ for both calibration data subsets (as stated earlier). The same observations hold for $f_{p_{cal}}$ and f_{φ} . For flow direction result uncertainty and total pressure result uncertainty the conclusion is unambiguous. Given a fixed amount of calibration data, flow direction and total pressure result uncertainty is reduced by using calibration data acquired at larger flow angles. For static pressure result uncertainty the comparison of $h_{p_{cal}}$ was more complicated. Values of $h_{p_{cal}}$ at large flow angles were less for the large flow angle calibration data set, as was expected, but $h_{p_{cal}}(0,0)$ was less for the small flow angle calibration data set. This suggests that static pressure result uncertainty is improved in the region where the calibration measurements are concentrated.

The major results of the uncertainty analysis are summarized below:

1. The uncertainty of five-hole probe results (e.g., total pressure, static pressure and flow direction) are shown to depend on the product of three measurand uncertainty parameters

and their corresponding influence functions. The measurand and uncertainty parameters quantify the uncertainty of the underlying calibration and experimental measurands.

2. For modest flow angles, most or all flow direction result uncertainty and total pressure result uncertainty comes from uncertainty in the experimental pressure measurands.
3. Total and static pressure result uncertainty can not be less than experimental pressure measurand uncertainty.
4. For modest flow angles, static pressure result uncertainty is necessarily greater than total pressure result uncertainty.
5. Result uncertainty may be reduced by reducing either the measurand uncertainty parameters or their influence functions. The measurand uncertainty parameters may be reduced by either using instruments with less measurement uncertainty or by using repeated measurements.
6. To reduce the three measurand uncertainty influence functions corresponding to experimental pressure measurand uncertainty requires modifying the probe geometry. For modest flow angles, flow direction result uncertainty can be reduced by increasing the angle of the openings of the four outer tubes. For modest flow angles, the total and static pressure result uncertainty coming from experimental pressure measurand uncertainty can not be reduced.
7. To reduce the four measurand uncertainty influence functions corresponding to calibration pressure and flow direction measurand uncertainty requires modifying the calibration procedure. The influence functions can be reduced by approximately one-half by increasing the amount of calibration data acquired by a factor of four.
8. In general, flow direction and total pressure result uncertainty may be reduced by acquiring calibration data at larger flow angles. However, this is not generally true for static pressure result uncertainty.

THE FIVE-HOLE PROBE RAKE

Motivation

The five-hole probe rake is built for use in NASA Lewis'

IFMF. This facility is schematically illustrated in Figure 11. The test section Mach number range is between 0.0 and 0.8 with corresponding mass flow rates between 0 and about 16 lbs/sec. Details concerning the operations and capabilities of the IFMF may be found in Porro *et al.* (1991). The IFMF is currently being used to test various inlet diffuser designs. These diffuser geometries possess high degrees of streamwise curvature and large changes in cross-sectional area providing a catalyst for strong secondary flows and attendant boundary layer flow separations. In the past, the resolution of these three-dimensional velocity fields was accomplished with a single five-hole probe traversed in the cross plane of the test section exit duct. The time required for a complete survey was considerable. As a means of saving time, the five-hole probe technique was extended to a rake arrangement; this idea prompted by the common use of Pitot probe rakes for measurements of total pressure.

Geometry, Construction, and Calibration

The rake probe is illustrated schematically in Figure 12. Ten individual five-hole probe tips are mounted one inch apart on the cylindrical stem spanning the tunnel diameter. Each tip is constructed from five 0.020" outer diameter stainless steel tubes silver brazed in the pattern indicated in Figure 12. After brazing, each tip face is ground to a 45° conical shape using a lathe and a fine grinding stone. A nominal tip diameter of 1/16" results from the brazing and grinding process. Each tip is individually calibrated following the previously outlined procedure. Probe symmetry is gauged by inspecting the calibration curves like those shown in Figures 3 through 5. Probe tips not meeting the desired level of symmetry are reground and recalibrated, or discarded.

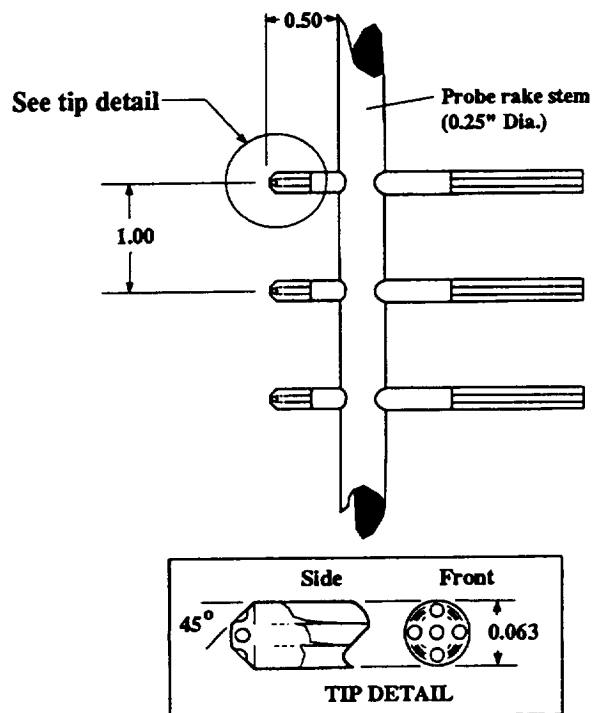


Figure 12 Rake probe geometry (Dimensions in inches)

Once mounted in the stem, the relative misalignment in pitch and yaw between consecutive tips is measured by traversing the full length of the rake through the calibration facility's open jet and recording the response of each tip.

Application and Results

Figure 13 illustrates the position of the rake probe inside the exit duct. One end of the rake probe is secured to a linear motion actuator which provides probe traversing in the radial coordinate, r . The other end of the probe also passes through the duct wall, and through a device similar to a linear bearing. This arrangement greatly reduces probe vibration and deflection when compared to the method of cantilevered support used with conventional probes. This can be a significant benefit when flow velocities are large or the distance to be spanned in a survey is large. Traversing in the circumferential coordinate, ζ , is accomplished by manually turning the duct with the rake probe and actuator attached. Surgical grade Tygon tubing (0.017" ID) is routed from the aft end of each probe tip, out of the exit duct, and to a series of Electro Scanning Pressure (ESP) transducer modules located in the facility. Probe pressures are recorded by NASA Lewis' ESCORT data acquisition system. The collected pressure data are transferred from storage on the ESCORT Scientific VAX cluster to Sun workstations where the reductions to velocities are performed.

Figure 14 illustrates transverse velocity components as determined by the rake probe at the exit plane of an S-duct, which is the current inlet diffuser model undergoing testing at the IFMF. The grid resolution is $\Delta r = 0.25"$, $\Delta \zeta = 10^\circ$. The local Mach number is approximately 0.4 and the total conditions are approximately atmospheric. Figure 15 is the corresponding result obtained with a single five-hole probe (Wellborn *et al.*, 1992). The only

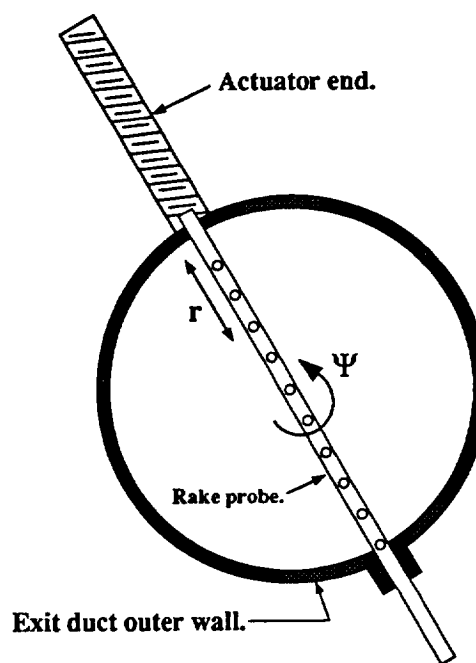


Figure 13 Rake probe actuation

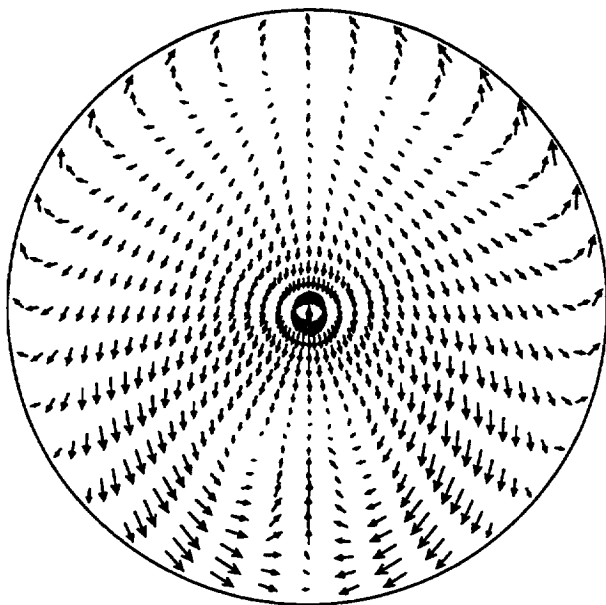


Figure 14 Transverse velocity components at the diffusing S-duct exit plane as measured by the rake probe

significant difference between Figures 14 and 15 is the time required to collect the data. The data illustrated in Figure 14 was collected in less than 5% of the time required for Figure 15. Use of the rake allows a substantial reduction in time and effort for the researchers at NASA Lewis' IFMF.

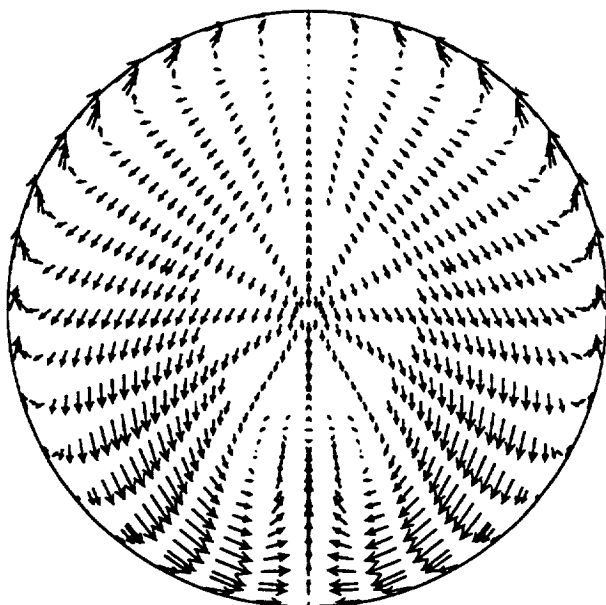


Figure 15 Transverse velocity components at the diffusing S-duct exit plane as measured by a conventional five-hole probe (yaw-nulling method)

SUMMARY

The large data sets associated with the use of a rake of five-hole probes provides the motivation for a novel algorithm of five-hole probe calibration and data reduction. In this algorithm four pressure coefficients are defined and related to flow angles through Taylor's series. Probe tip symmetries are used to reduced the number of series coefficients from sixty to thirteen. Laboratory calibrating and testing of individual five-hole probe tips verifies the validity and accuracy of the algorithm. In data reduction, the algorithm allows a much faster conversion of pressure to velocities, making the rake arrangement of five-hole tips a practical expedient to acquiring three-component velocity data sets in duct flow research.

An analytical treatment of the propagation of uncertainty in five-hole probe measurement was conducted. The uncertainty analysis determined the dependence of the result uncertainty on the uncertainty of all underlying experimental and calibration measurands and revealed details about the relationships between probe geometry, calibration, data reduction and result uncertainty. This study outlines a general procedure that other researchers may use to determine five-hole probe result uncertainty and provides guidance to improve measurement technique.

The ability to measure total and static pressure (hence velocity magnitude) and flow direction with a five-hole probe is well established. Recently we have constructed a rake of five-hole probe tips that operates in a non-nulling mode. Current non-nulling five-hole probe calibration and data reduction procedures typically involve complex interpolative algorithms. Development of the new algorithm makes the rake probe practical to use. The new algorithm uses two components of the unit vector in the flow direction instead of pitch and yaw angles as variables as well as probe tip symmetries to greatly simplifying both calibration and data reduction. In data reduction, total pressure, static pressure, and flow direction are calculated directly, without tables, spline network interpolation, or additional approximations. The result is a much faster reduction to velocities, making a rake probe arrangement of five-hole tips a practical expedient in duct flow research.

ACKNOWLEDGMENTS

We are grateful to Mr. S. Wellborn for the assistance he provided in the initial stages of this project, and to Mr. E. Abbey for his insights.

REFERENCES

- Rood, E. P. and Telionis, D. P., "Editorial," *Journal of Fluids Engineering*, Vol. 113, Sept. 1991, p. 313.
- Sutton, G. W., "Editorial Policy Statement on Numerical Accuracy and Experimental Uncertainty," *AIAA Journal*, Vol. 32, Jan. 1994, p. 3.
- Moffat, R. J., "Contributions to the Theory of Single-Sample Uncertainty Analysis," *Journal of Fluid Engineering*, Vol. 104, June 1982, pp. 250-258.

Bryer, D. W. and Pankhurst, R. C., *Pressure-Probe Methods for Determining Wind Speed and Flow Direction*, Her Majesty's Stationary Office, London, England, 1971.

Treaster, A. L. and Yocum, A. M., "The Calibration and Application of Five-hole Probes," *ISA Transactions*, Vol. 18, 1979, pp. 23-34.

Dudzinski, T. J. and Krause, L. N., "Flow-Direction Measurements with Fixed-Position Probes," NASA TM X-1904, Oct. 1969.

Lagrani, P. M., Singer, B. A., and Baun, L. R., "Miniature Five-Hole Pressure Probe for Measurement of Three Mean Ve-

locity Components in Low-Speed Flows," *Journal of Physics. E: Scientific Instruments*, Vol. 22, Oct. 1989.

Kline, S. J., "The Purposes of Uncertainty Analysis," *Journal of Fluid Engineering*, Vol. 107, June 1985, pp. 153-160.

Porro, A. R., Hingst, W. R., Wasserbauer, C. A., and Andrews, T. B., "The NASA Lewis Research Center Internal Fluid Mechanics Facility," NASA TM 105187, Sept. 1991.

Wellborn, S. R., Reichert, B. A., and Okiishi, T. H., "An Experimental Investigation of the Flow in a Diffusing S-Duct," AIAA Paper 92-3622, 1992. (Also NASA TM 105809).

APPENDIX CALIBRATION AND DATA REDUCTION

The coordinates of the i th probe opening (measured relative to the probe coordinate system) is $\mathbf{x}_i = (x_i, y_i, z_i)$. Because of probe xz -plane symmetry the following transformations are valid

$$\begin{aligned} T_y(\mathbf{x}_1) &= \mathbf{x}_1 \\ T_y(\mathbf{x}_2) &= \mathbf{x}_4 \\ T_y(\mathbf{x}_3) &= \mathbf{x}_3 \\ T_y(\mathbf{x}_4) &= \mathbf{x}_2 \\ T_y(\mathbf{x}_5) &= \mathbf{x}_5 \end{aligned}$$

where $T_y : (x, y, z) \rightarrow (x, -y, z)$.¹ For xy -plane symmetry the following transformations are valid

$$\begin{aligned} T_z(\mathbf{x}_1) &= \mathbf{x}_3 \\ T_z(\mathbf{x}_2) &= \mathbf{x}_2 \\ T_z(\mathbf{x}_3) &= \mathbf{x}_1 \\ T_z(\mathbf{x}_4) &= \mathbf{x}_4 \\ T_z(\mathbf{x}_5) &= \mathbf{x}_5 \end{aligned}$$

where $T_z : (x, y, z) \rightarrow (x, y, -z)$. Likewise, for 90° rotational symmetry about the x -axis the following transformations are valid

$$\begin{aligned} T_{90}(\mathbf{x}_1) &= \mathbf{x}_4 \\ T_{90}(\mathbf{x}_2) &= \mathbf{x}_1 \\ T_{90}(\mathbf{x}_3) &= \mathbf{x}_2 \\ T_{90}(\mathbf{x}_4) &= \mathbf{x}_3 \\ T_{90}(\mathbf{x}_5) &= \mathbf{x}_5 \end{aligned}$$

where $T_{90} : (x, y, z) \rightarrow (x, z, -y)$.

Consider a five-hole probe in a steady, uniform air flow. The boundary conditions that define the flow field are the free stream conditions at a distance well upstream of the probe. They are the free stream velocity $\mathbf{V}_\infty = (U_\infty, V_\infty, W_\infty)$ (measured relative to the probe coordinate system) and the free stream pressure p_∞ . For given free stream conditions there is a functional relationship between spatial coordinates and velocity and pressure, $\mathbf{V} : (x, y, z) \rightarrow (U, V, W)$, $P : (x, y, z) \rightarrow p$ and $P_0 : (x, y, z) \rightarrow p_0$. The pressure sensed by the i th probe opening is $p_i = p(\mathbf{x}_i)$.

Because of xz -plane symmetry and the invariance of the equations of motion $T_y \circ \mathbf{V} \circ T_y$ ² and $P \circ T_y$ are the velocity and pressure fields defined by the free stream conditions $T_y \circ \mathbf{V}_\infty$ and p_∞ . This requires

$$\begin{aligned} p_1 &= p(\mathbf{x}_1) = P \circ T_y(\mathbf{x}_1) \\ p_2 &= p(\mathbf{x}_2) = P \circ T_y(\mathbf{x}_4) \\ p_3 &= p(\mathbf{x}_3) = P \circ T_y(\mathbf{x}_3) \\ p_4 &= p(\mathbf{x}_4) = P \circ T_y(\mathbf{x}_2) \\ p_5 &= p(\mathbf{x}_5) = P \circ T_y(\mathbf{x}_5) \end{aligned}$$

The expression $P \circ T_y(\mathbf{x}_i)$ is interpreted as p_i for the free stream conditions $T_y \circ \mathbf{V}_\infty$ and p_∞ . For instance p_2 for free stream conditions \mathbf{V}_∞ and p_∞ equals p_4 for free stream conditions $T_y \circ \mathbf{V}_\infty$ and p_∞ . Thinking of the probe pressures as functions of free stream conditions then

$$\begin{aligned} p_1(U_\infty, V_\infty, W_\infty, p_\infty) &= p_1(U_\infty, -V_\infty, W_\infty, p_\infty) \\ p_2(U_\infty, V_\infty, W_\infty, p_\infty) &= p_4(U_\infty, -V_\infty, W_\infty, p_\infty) \\ p_3(U_\infty, V_\infty, W_\infty, p_\infty) &= p_3(U_\infty, -V_\infty, W_\infty, p_\infty) \\ p_4(U_\infty, V_\infty, W_\infty, p_\infty) &= p_2(U_\infty, -V_\infty, W_\infty, p_\infty) \\ p_5(U_\infty, V_\infty, W_\infty, p_\infty) &= p_5(U_\infty, -V_\infty, W_\infty, p_\infty) \end{aligned}$$

For xy -plane symmetry $T_z \circ \mathbf{V} \circ T_z$ and $P \circ T_z$ are the velocity and pressure fields defined by the free stream conditions $T_z \circ \mathbf{V}_\infty$ and p_∞ . Therefore

$$\begin{aligned} p_1 &= p(\mathbf{x}_1) = P \circ T_z(\mathbf{x}_3) \\ p_2 &= p(\mathbf{x}_2) = P \circ T_z(\mathbf{x}_2) \\ p_3 &= p(\mathbf{x}_3) = P \circ T_z(\mathbf{x}_1) \\ p_4 &= p(\mathbf{x}_4) = P \circ T_z(\mathbf{x}_4) \\ p_5 &= p(\mathbf{x}_5) = P \circ T_z(\mathbf{x}_5) \end{aligned}$$

and

$$\begin{aligned} p_1(U_\infty, V_\infty, W_\infty, p_\infty) &= p_3(U_\infty, V_\infty, -W_\infty, p_\infty) \\ p_2(U_\infty, V_\infty, W_\infty, p_\infty) &= p_2(U_\infty, V_\infty, -W_\infty, p_\infty) \\ p_3(U_\infty, V_\infty, W_\infty, p_\infty) &= p_1(U_\infty, V_\infty, -W_\infty, p_\infty) \\ p_4(U_\infty, V_\infty, W_\infty, p_\infty) &= p_4(U_\infty, V_\infty, -W_\infty, p_\infty) \\ p_5(U_\infty, V_\infty, W_\infty, p_\infty) &= p_5(U_\infty, V_\infty, -W_\infty, p_\infty) \end{aligned}$$

For 90° rotational symmetry $T_{90} \circ \mathbf{V} \circ T_{90}$ and $P \circ T_{90}$ are the velocity and pressure fields defined by the free stream conditions $T_{90} \circ \mathbf{V}_\infty$ and p_∞ . Therefore

$$\begin{aligned} p_1 &= p(\mathbf{x}_1) = P \circ T_{90}(\mathbf{x}_2) \\ p_2 &= p(\mathbf{x}_2) = P \circ T_{90}(\mathbf{x}_3) \\ p_3 &= p(\mathbf{x}_3) = P \circ T_{90}(\mathbf{x}_4) \\ p_4 &= p(\mathbf{x}_4) = P \circ T_{90}(\mathbf{x}_1) \\ p_5 &= p(\mathbf{x}_5) = P \circ T_{90}(\mathbf{x}_5) \end{aligned}$$

and

$$\begin{aligned} p_1(U_\infty, V_\infty, W_\infty, p_\infty) &= p_2(U_\infty, W_\infty, -V_\infty, p_\infty) \\ p_2(U_\infty, V_\infty, W_\infty, p_\infty) &= p_3(U_\infty, W_\infty, -V_\infty, p_\infty) \\ p_3(U_\infty, V_\infty, W_\infty, p_\infty) &= p_4(U_\infty, W_\infty, -V_\infty, p_\infty) \\ p_4(U_\infty, V_\infty, W_\infty, p_\infty) &= p_1(U_\infty, W_\infty, -V_\infty, p_\infty) \\ p_5(U_\infty, V_\infty, W_\infty, p_\infty) &= p_5(U_\infty, W_\infty, -V_\infty, p_\infty) \end{aligned}$$

To develop our calibration and data reduction procedure, five pressure coefficients, one for each probe opening, are defined by Equation 1. These coefficients are not used for calibration and data reduction, but they help analyze concepts relating to probe symmetry that are essential to our calibration and data reduction scheme. Since p_i may be considered a function of $U_\infty, V_\infty, W_\infty, p_\infty$ then so is the coefficient Cp_i , a function of these four quantities. Like the pressure coefficients described previously the pressure coefficients given by Equation 1 are insensitive to a range of Reynolds and subsonic Mach numbers and depend on flow direction only. Therefore, Cp_i is a function of the unit vectors $u_\infty, v_\infty, w_\infty$. Since this is a unit vector, only two components are independent, so with the restriction $u_\infty > 0$ and dropping the ∞ subscript for

¹ The function T_y is sometimes called a flip. The domain of T_y is not necessarily physical space. For instance $T_y : (u, v, w) \rightarrow (u, -v, w)$.

² The notation \circ used here is the composition of two functions. For instance, for functions $f(x)$ and $g(x)$ then $f \circ g = f(g(x))$.

the sake of simplicity we say Cp_i is a function of v, w , as is shown in Equation 1.

$$Cp_i = \frac{p_i(U_\infty, V_\infty, W_\infty, p_\infty) - p_\infty}{p_{0,\infty} - p_\infty} \quad (1)$$

$$= Cp_i(v, w)$$

We may now state the probe symmetry rules in terms of the pressure coefficients Cp_i . For xz -plane symmetry

$$\begin{aligned} Cp_1(v, w) &= Cp_1(-v, w) \\ Cp_2(v, w) &= Cp_4(-v, w) \\ Cp_3(v, w) &= Cp_3(-v, w) \\ Cp_4(v, w) &= Cp_2(-v, w) \\ Cp_5(v, w) &= Cp_5(-v, w) \end{aligned}$$

For xy -plane symmetry

$$\begin{aligned} Cp_1(v, w) &= Cp_3(v, -w) \\ Cp_2(v, w) &= Cp_2(v, -w) \\ Cp_3(v, w) &= Cp_1(v, -w) \\ Cp_4(v, w) &= Cp_4(v, -w) \\ Cp_5(v, w) &= Cp_5(v, -w) \end{aligned}$$

For 90° rotational symmetry about the x -axis

$$\begin{aligned} Cp_1(v, w) &= Cp_2(w, -v) \\ Cp_2(v, w) &= Cp_3(w, -v) \\ Cp_3(v, w) &= Cp_4(w, -v) \\ Cp_4(v, w) &= Cp_1(w, -v) \\ Cp_5(v, w) &= Cp_5(w, -v) \end{aligned}$$

Proofs of the rules stated above are very straightforward. For instance the proof that $Cp_1(v, w) = Cp_1(-v, w)$ is

$$\begin{aligned} Cp_1(v, w) &= \frac{p_1(U_\infty, V_\infty, W_\infty, p_\infty) - p_\infty}{p_{0,\infty} - p_\infty} \\ &= \frac{p_1(U_\infty, -V_\infty, W_\infty, p_\infty) - p_\infty}{p_{0,\infty} - p_\infty} \\ &= Cp_1(-v, w) \end{aligned}$$

The remaining proofs are nearly identical and are not repeated.

The pressure coefficients used in calibration and data reduction and given by Equations 1, 3 and 4 can also be defined in terms of the five pressure coefficients, as shown below.

$$Cp_{avg} = \frac{1}{4}(Cp_1 + Cp_2 + Cp_3 + Cp_4)$$

$$Cp_v = \frac{Cp_2 - Cp_4}{Cp_5 - Cp_{avg}}$$

$$Cp_w = \frac{Cp_3 - Cp_1}{Cp_5 - Cp_{avg}}$$

The probe symmetry rules for the coefficients Cp_{avg} , Cp_v and Cp_w are

$$\begin{aligned} Cp_{avg}(v, w) &= Cp_{avg}(-v, w) \\ Cp_{avg}(v, w) &= Cp_{avg}(v, -w) \\ Cp_{avg}(v, w) &= Cp_{avg}(w, -v) \end{aligned}$$

$$\begin{aligned} Cp_v(v, w) &= -Cp_v(-v, w) \\ Cp_v(v, w) &= Cp_v(v, -w) \\ Cp_w(v, w) &= Cp_w(-v, w) \\ Cp_w(v, w) &= -Cp_w(v, -w) \\ Cp_v(v, w) &= Cp_w(w, -v) \end{aligned}$$

Proofs for these rules are stated below

$$\begin{aligned} Cp_{avg}(v, w) &= \frac{1}{4}(Cp_1(v, w) + Cp_2(v, w) \\ &\quad + Cp_3(v, w) + Cp_4(v, w)) \\ &= \frac{1}{4}(Cp_1(-v, w) + Cp_4(-v, w) \\ &\quad + Cp_3(-v, w) + Cp_2(-v, w)) \\ &= Cp_{avg}(-v, w) \end{aligned}$$

$$\begin{aligned} Cp_{avg}(v, w) &= \frac{1}{4}(Cp_1(v, w) + Cp_2(v, w) \\ &\quad + Cp_3(v, w) + Cp_4(v, w)) \\ &= \frac{1}{4}(Cp_3(v, -w) + Cp_2(v, -w) \\ &\quad + Cp_1(v, -w) + Cp_4(v, -w)) \\ &= Cp_{avg}(v, -w) \end{aligned}$$

$$\begin{aligned} Cp_{avg}(v, w) &= \frac{1}{4}(Cp_1(v, w) + Cp_2(v, w) \\ &\quad + Cp_3(v, w) + Cp_4(v, w)) \\ &= \frac{1}{4}(Cp_2(w, -v) + Cp_3(w, -v) \\ &\quad + Cp_4(w, -v) + Cp_1(w, -v)) \\ &= Cp_{avg}(w, -v) \end{aligned}$$

$$\begin{aligned} Cp_v(v, w) &= \frac{Cp_2(v, w) - Cp_4(v, w)}{Cp_5(v, w) - Cp_{avg}(v, w)} \\ &= \frac{Cp_4(-v, w) - Cp_2(-v, w)}{Cp_5(-v, w) - Cp_{avg}(-v, w)} \\ &= -\frac{Cp_2(-v, w) - Cp_4(-v, w)}{Cp_5(-v, w) - Cp_{avg}(-v, w)} \\ &= -Cp_v(-v, w) \end{aligned}$$

$$\begin{aligned} Cp_v(v, w) &= \frac{Cp_2(v, w) - Cp_4(v, w)}{Cp_5(v, w) - Cp_{avg}(v, w)} \\ &= \frac{Cp_2(v, -w) - Cp_4(v, -w)}{Cp_5(v, -w) - Cp_{avg}(v, -w)} \\ &= Cp_v(v, -w) \end{aligned}$$

$$\begin{aligned} Cp_w(v, w) &= \frac{Cp_3(v, w) - Cp_1(v, w)}{Cp_5(v, w) - Cp_{avg}(v, w)} \\ &= \frac{Cp_3(-v, w) - Cp_1(-v, w)}{Cp_5(-v, w) - Cp_{avg}(-v, w)} \\ &= Cp_w(-v, w) \end{aligned}$$

$$\begin{aligned}
Cp_w(v, w) &= \frac{Cp_3(v, w) - Cp_1(v, w)}{Cp_5(v, w) - Cp_{avg}(v, w)} \\
&= \frac{Cp_1(v, -w) - Cp_3(v, -w)}{Cp_5(v, -w) - Cp_{avg}(v, -w)} \\
&= -\frac{Cp_3(v, -w) - Cp_1(v, -w)}{Cp_5(v, -w) - Cp_{avg}(v, -w)} \\
&= -Cp_w(v, -w)
\end{aligned}$$

$$\begin{aligned}
Cp_v(v, w) &= \frac{Cp_2(v, w) - Cp_4(v, w)}{Cp_5(v, w) - Cp_{avg}(v, w)} \\
&= \frac{Cp_3(w, -v) - Cp_1(w, -v)}{Cp_5(w, -v) - Cp_{avg}(w, -v)} \\
&= Cp_w(w, -v)
\end{aligned}$$

The symmetry rules for v and w as function of Cp_v and Cp_w are stated and proven below

$$\begin{aligned}
v(Cp_v, Cp_w) &= -v(-Cp_v, Cp_w) \\
v(Cp_v, Cp_w) &= v(Cp_v, -Cp_w) \\
w(Cp_v, Cp_w) &= w(-Cp_v, Cp_w) \\
w(Cp_v, Cp_w) &= -w(Cp_v, -Cp_w) \\
v(Cp_v, Cp_w) &= w(Cp_w, -Cp_v)
\end{aligned}$$

$$\begin{aligned}
v(Cp_v, Cp_w) &= v(Cp_v(v, w), Cp_w(v, w)) \\
&= v(Cp_v(v, -w), Cp_w(v, -w)) \\
&= v(Cp_v(v, w), -Cp_w(v, w)) \\
&= v(Cp_v, -Cp_w)
\end{aligned}$$

The proof that $w(Cp_v, Cp_w) = w(-Cp_v, Cp_w)$ is identical and is not repeated.

$$\begin{aligned}
v(Cp_v, Cp_w) &= v(Cp_v(v, w), Cp_w(v, w)) \\
&= -v(Cp_v(-v, w), Cp_w(-v, w)) \\
&= -v(-Cp_v(v, w), Cp_w(v, w)) \\
&= -v(-Cp_v, Cp_w)
\end{aligned}$$

The proof that $w(Cp_v, Cp_w) = -w(Cp_v, -Cp_w)$ is identical and is not repeated.

$$\begin{aligned}
v(Cp_v(v, w), Cp_w(v, w)) &= w(Cp_v(w, v), Cp_w(w, v)) \\
v(Cp_v, Cp_w) &= w(Cp_w(v, -w), Cp_v(v, -w)) \\
&= w(-Cp_w(v, w), Cp_v(v, w)) \\
&= w(-Cp_w, Cp_v) \\
&= w(Cp_w, Cp_v)
\end{aligned}$$

The symmetry rules for Cp_{avg} and Cp_5 as functions of Cp_v and Cp_w are stated and proven below.

$$\begin{aligned}
Cp_{avg}(Cp_v, Cp_w) &= Cp_{avg}(-Cp_v, Cp_w) \\
Cp_{avg}(Cp_v, Cp_w) &= Cp_{avg}(Cp_v, -Cp_w) \\
Cp_{avg}(Cp_v, Cp_w) &= Cp_{avg}(Cp_w, -Cp_v) \\
Cp_5(Cp_v, Cp_w) &= Cp_5(-Cp_v, Cp_w) \\
Cp_5(Cp_v, Cp_w) &= Cp_5(Cp_v, -Cp_w) \\
Cp_5(Cp_v, Cp_w) &= Cp_5(Cp_w, -Cp_v)
\end{aligned}$$

$$\begin{aligned}
Cp_{avg}(Cp_v, Cp_w) &= Cp_{avg}(Cp_v(v, w), Cp_w(v, w)) \\
&= Cp_{avg}(Cp_v(-v, w), Cp_w(-v, w)) \\
&= Cp_{avg}(-Cp_v(v, w), Cp_w(v, w)) \\
&= Cp_{avg}(-Cp_v, Cp_w)
\end{aligned}$$

The proofs that $Cp_{avg}(Cp_v, Cp_w) = Cp_{avg}(Cp_v, -Cp_w)$, $Cp_5(Cp_v, Cp_w) = Cp_5(-Cp_v, Cp_w)$ and $Cp_5(Cp_v, Cp_w) = Cp_5(Cp_v, -Cp_w)$ are identical and are not repeated.

$$\begin{aligned}
Cp_{avg}(Cp_v, Cp_w) &= Cp_{avg}(Cp_v(v, w), Cp_w(v, w)) \\
&= Cp_{avg}(Cp_w(w, -v), Cp_v(w, -v)) \\
&= Cp_{avg}(Cp_w, Cp_v) \\
&= Cp_{avg}(Cp_w, -Cp_v)
\end{aligned}$$

The proof that $Cp_5(Cp_v, Cp_w) = Cp_5(Cp_w, -Cp_v)$ is identical and is not repeated.

The consequence of the symmetry rules on the Taylor's series for Cp_{avg} and Cp_5 are stated and proven below

$$\begin{aligned}
a_{ij} &= 0, \quad i = 1, 3, 5, \dots \\
a_{ij} &= 0, \quad j = 1, 3, 5, \dots \\
a_{ij} &= a_{ji} \\
b_{ij} &= 0, \quad i = 1, 3, 5, \dots \\
b_{ij} &= 0, \quad j = 1, 3, 5, \dots \\
b_{ij} &= b_{ji}
\end{aligned}$$

$$\begin{aligned}
Cp_{avg}(Cp_v, Cp_w) &= a_{00} \\
&+ a_{10}Cp_v + a_{01}Cp_w \\
&+ a_{20}Cp_v^2 + a_{11}Cp_vCp_w + a_{02}Cp_w^2 \\
&+ a_{30}Cp_v^3 + a_{21}Cp_v^2Cp_w + a_{12}Cp_vCp_w^2 \\
&+ a_{03}Cp_w^3 \\
&+ a_{40}Cp_v^4 + a_{31}Cp_v^3Cp_w + a_{22}Cp_v^2Cp_w^2 \\
&+ a_{13}Cp_vCp_w^3 + a_{04}Cp_w^4 \\
&+ \dots
\end{aligned}$$

$$\begin{aligned}
Cp_{avg}(-Cp_v, Cp_w) &= a_{00} \\
&- a_{10}Cp_v + a_{01}Cp_w \\
&+ a_{20}Cp_v^2 - a_{11}Cp_vCp_w + a_{02}Cp_w^2 \\
&- a_{30}Cp_v^3 + a_{21}Cp_v^2Cp_w - a_{12}Cp_vCp_w^2 \\
&+ a_{03}Cp_w^3 \\
&+ a_{40}Cp_v^4 - a_{31}Cp_v^3Cp_w + a_{22}Cp_v^2Cp_w^2 \\
&- a_{13}Cp_vCp_w^3 + a_{04}Cp_w^4 \\
&+ \dots
\end{aligned}$$

$$\begin{aligned}
Cp_{avg}(Cp_v, Cp_w) - Cp_{avg}(-Cp_v, Cp_w) = \\
2a_{10}Cp_v \\
+ 2a_{11}Cp_vCp_w \\
+ 2a_{30}Cp_v^3 + 2a_{12}Cp_vCp_w^2 \\
+ 2a_{31}Cp_v^3Cp_w + 2a_{13}Cp_vCp_w^3 \\
+ \dots \\
= 0
\end{aligned}$$

Since $Cp_{avg}(Cp_v, Cp_w) - Cp_{avg}(-Cp_v, Cp_w) = 0$ for all Cp_v and Cp_w then all the coefficients a_{ij} where $i = 1, 3, 5, \dots$ are equal to zero. The proofs that $a_{ij} = 0$, $j = 1, 3, 5, \dots$, $b_{ij} = 0$, $i = 1, 3, 5, \dots$ and $b_{ij} = 0$, $j = 1, 3, 5, \dots$ are identical and are not repeated.

$$\begin{aligned}
Cp_{avg}(Cp_v, Cp_w) = a_{00} \\
+ a_{10}Cp_v + a_{01}Cp_w \\
+ a_{20}Cp_v^2 + a_{11}Cp_vCp_w + a_{02}Cp_w^2 \\
+ a_{30}Cp_v^3 + a_{21}Cp_v^2Cp_w + a_{12}Cp_vCp_w^2 \\
+ a_{03}Cp_w^3 \\
+ a_{40}Cp_v^4 + a_{31}Cp_v^3Cp_w + a_{22}Cp_v^2Cp_w^2 \\
+ a_{13}Cp_vCp_w^3 + a_{04}Cp_w^4 \\
+ \dots
\end{aligned}$$

$$\begin{aligned}
Cp_{avg}(Cp_w, Cp_v) = a_{00} \\
+ a_{10}Cp_w + a_{01}Cp_v \\
+ a_{20}Cp_w^2 + a_{11}Cp_wCp_v + a_{02}Cp_v^2 \\
+ a_{30}Cp_w^3 + a_{21}Cp_w^2Cp_v + a_{12}Cp_wCp_v^2 \\
+ a_{03}Cp_v^3 \\
+ a_{40}Cp_w^4 + a_{31}Cp_w^3Cp_v + a_{22}Cp_w^2Cp_v^2 \\
+ a_{13}Cp_wCp_v^3 + a_{04}Cp_v^4 \\
+ \dots
\end{aligned}$$

$$\begin{aligned}
Cp_{avg}(Cp_v, Cp_w) - Cp_{avg}(Cp_w, Cp_v) \\
= (a_{10} - a_{01})(Cp_v - Cp_w) \\
+ (a_{20} - a_{02})(Cp_v^2 - Cp_w^2) \\
+ (a_{30} - a_{03})(Cp_v^3 - Cp_w^3) \\
+ (a_{21} - a_{12})(Cp_v^2Cp_w - Cp_vCp_w^2) \\
+ (a_{40} - a_{04})(Cp_v^4 - Cp_w^4) \\
+ (a_{31} - a_{13})(Cp_v^3Cp_w - Cp_vCp_w^3) \\
+ \dots
\end{aligned}$$

Since $Cp_{avg}(Cp_v, Cp_w) - Cp_{avg}(Cp_w, Cp_v) = 0$ for all Cp_v and Cp_w then this requires $a_{ij} = a_{ji}$. The proof that $b_{ij} = b_{ji}$ is identical and is not repeated.

The consequence of the symmetry rules on the Taylor's series for v and w are stated and proven below

$$c_{ij} = 0, \quad i = 0, 2, 4, \dots$$

$$\begin{aligned}
c_{ij} &= 0, \quad j = 1, 3, 5, \dots \\
d_{ij} &= 0, \quad i = 1, 3, 5, \dots \\
d_{ij} &= 0, \quad j = 0, 2, 4, \dots \\
c_{ij} &= d_{ji}
\end{aligned}$$

$$\begin{aligned}
v(Cp_v, Cp_w) = c_{00} \\
+ c_{10}Cp_v + c_{01}Cp_w \\
+ c_{20}Cp_v^2 + c_{11}Cp_vCp_w + c_{02}Cp_w^2 \\
+ c_{30}Cp_v^3 + c_{21}Cp_v^2Cp_w + c_{12}Cp_vCp_w^2 \\
+ c_{03}Cp_w^3 \\
+ c_{40}Cp_v^4 + c_{31}Cp_v^3Cp_w + c_{22}Cp_v^2Cp_w^2 \\
+ c_{13}Cp_vCp_w^3 + c_{04}Cp_w^4 \\
+ \dots
\end{aligned}$$

$$\begin{aligned}
v(-Cp_v, Cp_w) = c_{00} \\
- c_{10}Cp_v + c_{01}Cp_w \\
+ c_{20}Cp_v^2 - c_{11}Cp_vCp_w + c_{02}Cp_w^2 \\
- c_{30}Cp_v^3 + c_{21}Cp_v^2Cp_w - c_{12}Cp_vCp_w^2 \\
+ c_{03}Cp_w^3 \\
+ c_{40}Cp_v^4 - c_{31}Cp_v^3Cp_w + c_{22}Cp_v^2Cp_w^2 \\
- c_{13}Cp_vCp_w^3 + c_{04}Cp_w^4 \\
+ \dots
\end{aligned}$$

$$\begin{aligned}
v(Cp_v, Cp_w) + v(-Cp_v, Cp_w) = \\
2c_{00} \\
+ 2c_{01}Cp_w \\
+ 2c_{20}Cp_v^2 + 2c_{02}Cp_w^2 \\
+ 2c_{21}Cp_v^2Cp_w + 2c_{03}Cp_w^3 \\
+ 2c_{40}Cp_v^4 + 2c_{22}Cp_v^2Cp_w^2 + 2c_{04}Cp_w^4 \\
+ \dots \\
= 0
\end{aligned}$$

Since $v(Cp_v, Cp_w) + v(-Cp_v, Cp_w) = 0$ for all Cp_v and Cp_w then all the coefficients c_{ij} where $i = 0, 2, 4, \dots$ are equal to zero. The proof that $d_{ij} = 0$, $j = 0, 2, 4, \dots$ is identical and is not repeated.

$$\begin{aligned}
v(Cp_v, Cp_w) = c_{00} \\
+ c_{10}Cp_v + c_{01}Cp_w \\
+ c_{20}Cp_v^2 + c_{11}Cp_vCp_w + c_{02}Cp_w^2 \\
+ c_{30}Cp_v^3 + c_{21}Cp_v^2Cp_w + c_{12}Cp_vCp_w^2 \\
+ c_{03}Cp_w^3 \\
+ c_{40}Cp_v^4 + c_{31}Cp_v^3Cp_w + c_{22}Cp_v^2Cp_w^2 \\
+ c_{13}Cp_vCp_w^3 + c_{04}Cp_w^4 \\
+ \dots
\end{aligned}$$

$$\begin{aligned}
v(Cp_v, -Cp_w) &= c_{00} \\
&+ c_{10}Cp_v - c_{01}Cp_w \\
&+ c_{20}Cp_v^2 - c_{11}Cp_vCp_w + c_{02}Cp_w^2 \\
&+ c_{30}Cp_v^3 - c_{21}Cp_v^2Cp_w + c_{12}Cp_vCp_w^2 \\
&\quad - c_{03}Cp_w^3 \\
&+ c_{40}Cp_v^4 - c_{31}Cp_v^3Cp_w + c_{22}Cp_v^2Cp_w^2 \\
&\quad - c_{13}Cp_vCp_w^3 + c_{04}Cp_w^4 \\
&+ \dots \\
v(Cp_v, Cp_w) - v(Cp_v, -Cp_w) &= \\
&+ 2c_{01}Cp_w \\
&+ 2c_{11}Cp_vCp_w \\
&+ 2c_{21}Cp_v^2Cp_w + 2c_{03}Cp_w^3 \\
&+ 2c_{31}Cp_v^3Cp_w + 2c_{13}Cp_vCp_w^3 + \\
&+ \dots \\
&= 0
\end{aligned}$$

Since $v(Cp_v, Cp_w) - v(Cp_v, -Cp_w) = 0$ for all Cp_v and Cp_w then all the coefficients c_{ij} where $j = 1, 3, 5, \dots$ are equal to zero. The proof that $d_{ij} = 0$, $j = 0, 2, 4, \dots$ is identical and is not repeated.

$$\begin{aligned}
v(Cp_v, Cp_w) &= c_{00} \\
&+ c_{10}Cp_v + c_{01}Cp_w \\
&+ c_{20}Cp_v^2 + c_{11}Cp_vCp_w + c_{02}Cp_w^2 \\
&+ c_{30}Cp_v^3 + c_{21}Cp_v^2Cp_w + c_{12}Cp_vCp_w^2 \\
&\quad + c_{03}Cp_w^3 \\
&+ c_{40}Cp_v^4 + c_{31}Cp_v^3Cp_w + c_{22}Cp_v^2Cp_w^2 \\
&\quad + c_{13}Cp_vCp_w^3 + c_{04}Cp_w^4 \\
&+ \dots
\end{aligned}$$

$$\begin{aligned}
w(Cp_w, Cp_v) &= d_{00} \\
&+ d_{10}Cp_w + d_{01}Cp_v \\
&+ d_{20}Cp_w^2 + d_{11}Cp_wCp_v + d_{02}Cp_v^2 \\
&+ d_{30}Cp_w^3 + d_{21}Cp_w^2Cp_v + d_{12}Cp_wCp_v^2 \\
&\quad + d_{03}Cp_v^3 \\
&+ d_{40}Cp_w^4 + d_{31}Cp_w^3Cp_v + d_{22}Cp_w^2Cp_v^2 \\
&\quad + d_{13}Cp_wCp_v^3 + d_{04}Cp_v^4 \\
&+ \dots
\end{aligned}$$

$$\begin{aligned}
v(Cp_v, Cp_w) - w(Cp_w, Cp_v) &= \\
&= +(c_{10} - d_{01})(Cp_v - Cp_w) \\
&+ (c_{20} - d_{02})(Cp_v^2 - Cp_w^2) \\
&+ (c_{30} - d_{03})(Cp_v^3 - Cp_w^3) \\
&+ (c_{21} - d_{12})(Cp_v^2Cp_w - Cp_vCp_w^2) \\
&+ (c_{40} - d_{04})(Cp_v^4 - Cp_w^4) \\
&+ (c_{31} - d_{13})(Cp_v^3Cp_w - Cp_vCp_w^3) \\
&+ \dots
\end{aligned}$$

Since $v(Cp_v, Cp_w) - w(Cp_w, Cp_v) = 0$ for all Cp_v and Cp_w then this requires $c_{ij} = d_{ji}$.

REPORT DOCUMENTATION PAGEForm Approved
OMB No. 0704-0188

Public reporting burden for this collection of information is estimated to average 1 hour per response, including the time for reviewing instructions, searching existing data sources, gathering and maintaining the data needed, and completing and reviewing the collection of information. Send comments regarding this burden estimate or any other aspect of this collection of information, including suggestions for reducing this burden, to Washington Headquarters Services, Directorate for Information Operations and Reports, 1215 Jefferson Davis Highway, Suite 1204, Arlington, VA 22202-4302, and to the Office of Management and Budget, Paperwork Reduction Project (0704-0188), Washington, DC 20503.

1. AGENCY USE ONLY (Leave blank)		2. REPORT DATE September 1994	3. REPORT TYPE AND DATES COVERED Technical Memorandum	
4. TITLE AND SUBTITLE A New Algorithm for Five-Hole Probe Calibration, Data Reduction, and Uncertainty Analysis			5. FUNDING NUMBERS WU-505-62-52	
6. AUTHOR(S) Bruce A. Reichert and Bruce J. Wendt				
7. PERFORMING ORGANIZATION NAME(S) AND ADDRESS(ES) National Aeronautics and Space Administration Lewis Research Center Cleveland, Ohio 44135-3191			8. PERFORMING ORGANIZATION REPORT NUMBER E-8319	
9. SPONSORING/MONITORING AGENCY NAME(S) AND ADDRESS(ES) National Aeronautics and Space Administration Washington, D.C. 20546-0001			10. SPONSORING/MONITORING AGENCY REPORT NUMBER NASA TM-106458	
11. SUPPLEMENTARY NOTES Bruce A. Reichert, NASA Lewis Research Center; and Bruce J. Wendt, National Research Council-NASA Resident Research Associate at Lewis Research Center. Responsible person, Bruce A. Reichert, organization code 2660, (216) 433-8397.				
12a. DISTRIBUTION/AVAILABILITY STATEMENT Unclassified - Unlimited Subject Category 02			12b. DISTRIBUTION CODE	
13. ABSTRACT (Maximum 200 words) A new algorithm for five-hole probe calibration and data reduction using a non-nulling method is developed. The significant features of the algorithm are: 1) two components of the unit vector in the flow direction replace pitch and yaw angles as flow direction variables, and 2) symmetry rules are developed that greatly simplify Taylor's series representations of the calibration data. In data reduction, four pressure coefficients allow total pressure, static pressure, and flow direction to be calculated directly. The new algorithm's simplicity permits an analytical treatment of the propagation of uncertainty in five-hole probe measurement. The objectives of the uncertainty analysis are to quantify uncertainty of five-hole probe results (e.g., total pressure, static pressure, and flow direction) and determine the dependence of the result uncertainty on the uncertainty of all underlying experimental and calibration measurands. This study outlines a general procedure that other researchers may use to determine five-hole probe result uncertainty and provides guidance to improve measurement technique. The new algorithm is applied to calibrate and reduce data from a rake of five-hole probes. Here, ten individual probes are mounted on a single probe shaft and used simultaneously. Use of this probe is made practical by the simplicity afforded by this algorithm.				
14. SUBJECT TERMS Flow measurement; Pneumatic probes; Velocity measurement; Pressure measurement; Error analysis; Uncertainty analysis			15. NUMBER OF PAGES 20	
			16. PRICE CODE A03	
17. SECURITY CLASSIFICATION OF REPORT Unclassified	18. SECURITY CLASSIFICATION OF THIS PAGE Unclassified	19. SECURITY CLASSIFICATION OF ABSTRACT Unclassified	20. LIMITATION OF ABSTRACT	